

**Comparison of Linear Regression and a Probabilistic Neural Network
to Predict Porosity from 3-D seismic attributes in Lower Brushy
Canyon Channeled Sandstones, Southeast New Mexico**

by
Dan Leiphart

Submitted in partial fulfillment of the requirements for
the degree of Masters of Science in Geology

New Mexico Institute of Mining and Technology
Socorro, New Mexico
June 2000

PREFACE

This thesis is written in manuscript form appropriate for submission to a scientific journal. Consequently, the content has been condensed so as to omit repetitious and detailed material from the methods and results sections. Details of procedures are given in the appendices at the end of the paper.

TABLE OF CONTENTS

| | |
|--|------|
| Preface ----- | ii |
| Table of Contents ----- | iii |
| List of Figures ----- | iv |
| List of Tables ----- | vi |
| List of Appendices ----- | vii |
| Acknowledgements ----- | viii |
| Abstract ----- | ix |
| Introduction ----- | 1 |
| Geologic Setting ----- | 2 |
| Materials and Methods ----- | 3 |
| Stratigraphy ----- | 5 |
| Lower Brushy Canyon Picks ----- | 6 |
| Seismic Horizons ----- | 8 |
| Discussion – Stratigraphy ----- | 10 |
| Seismic Attribute Study ----- | 12 |
| Methods ----- | 12 |
| Results – Attribute Study ----- | 14 |
| Discussion ----- | 24 |
| Analysis ----- | 28 |
| Conclusion ----- | 29 |
| References ----- | 31 |
| Appendix 1 ----- | 34 |
| Stratigraphic Interpretations ----- | 34 |
| Synthetic Seismograms ----- | 38 |
| Seismic Interpretations ----- | 42 |
| Seismic Attribute Analyses ----- | 43 |
| Appendix 2 ----- | 50 |
| Definition of the PNN ----- | 50 |
| Procedures in Application and Methodology of the PNN ----- | 51 |

LIST OF FIGURES

| | |
|---|----|
| Figure 1: Regional paleogeographic map showing the Permian Basin complex ---- | 2 |
| Figure 2: Sample log through the lower Brushy Canyon in this study area ----- | 5 |
| Figure 3: NW-SE stratigraphic cross-section through the study area datumed at the lower Brushy Canyon ----- | 6 |
| Figure 4: Isopach maps for each of the units in the lower Brushy Canyon Formation | 7 |
| Figure 5: West - east seismic transect near the center of the study area ----- | 9 |
| Figure 6: Depth-converted structure map of the top of the Bone Spring Formation calculated from the seismic data ----- | 11 |
| Figure 7: Application of the linear regression method to predicting porosity ----- | 17 |
| Figure 8: Cross-plot of the linear regression model results ----- | 18 |
| Figure 9: Application of the probabilistic neural network to predicting porosity - | 19 |
| Figure 10: Cross-plot of the PNN results ----- | 20 |
| Figure 11: Linear regression predicted porosity map of the entire Unit C interval --- | 21 |
| Figure 12: Linear regression predicted porosity map of units A through D interval - | 22 |
| Figure 13: PNN predicted porosity map of the entire Unit C interval ----- | 23 |
| Figure 14: PNN predicted porosity map of stratigraphic units A through D ----- | 24 |
| Figure 15: Comparison of the Unit D isopach (Figure 4D) with a contour interval of 10 feet and the smoothed average predicted porosity map of the entire Unit D time window using the PNN model ----- | 25 |
| Figure 16: PNN-based average predicted porosity map of the entire units A through D time window with cumulative basal Brushy Canyon production data overlain ----- | 28 |

| | |
|--|----|
| Figure 17: Locations of the 11 wells used in the multiattribute study ----- | 36 |
| Figure 18: Well logs and log-based lithology column of a well southeast of center in the study area ----- | 37 |
| Figure 19: A west – east cross-section showing basic lower Brushy Canyon stratigraphy ----- | 39 |
| Figure 20: A synthetic seismogram tying the well log to the seismic data ----- | 43 |
| Figure 21: Time-structure map the lower Brushy Canyon Formation as interpreted in the seismic volume ----- | 44 |
| Figure 22: Time-structure map of the top of the Bone Spring horizon in the seismic data ----- | 45 |
| Figure 23: Isochron of the lower Brushy Canyon interval in the seismic volume ----- | 45 |
| Figure 24: Individual cross-plots of attribute vs. neutron porosity for each of the seven attributes used in the analysis ----- | 46 |

LIST OF TABLES

| | |
|--|----|
| Table 1: List of the seismic attributes chosen and ranked by step-wise regression and the associated application error (includes all 11 wells) and validation error (excludes one well at a time as the target well) ----- | 14 |
| Table 2: A list of eight wells not used in the multiattribute study whose average Unit C porosity is known and tested against the predictions of the regression and the PNN models ----- | 25 |
| Table 3: Time/depth pairs for every lower Brushy Canyon stratigraphic pick for each of the 11 wells in the multiattribute study ----- | 35 |
| Table 4: List of the correlation coefficients and time windows for each of the wells used in the multiattribute study ----- | 41 |
| Table 5: List of the weights applied to each attribute ----- | 48 |
| Table 6: List of the sigma values for each attribute ----- | 51 |

LIST OF APPENDICES

| | |
|---|----|
| Appendix 1: Procedures, Methods, and Applications in Geologic Interpretations ----- | 34 |
| Appendix 2: Definition, Application and Methodology of the PNN ----- | 50 |

ACKNOWLEDGEMENTS

We would like to thank Pogo Producing Company and Burlington Resources for the well database and the 3-D seismic volume. The New Mexico Bureau of Mines and Mineral Research provided the funding for this project. All stratigraphic and seismic interpretations were done on Landmark Graphics Corporation and Hampson and Russell software. Also, we would like to thank committee members Drs. Bruce Hart, Peter Mozley, and Dave Johnson, as well as Robin Pearson for her assistance in understanding the capabilities of the software.

ABSTRACT

The Lower Brushy Canyon Formation of the Delaware Basin consists of a series of overlying sand-filled channels and associated fans separated by laterally extensive organic siltstone and carbonate interbeds. This laterally and vertically complex geology creates the need for precise inter-well estimation of reservoir properties.

In this paper we integrate wireline log and 3-D seismic data in order to directly predict porosity in the area of an existing oil field in southeast New Mexico. The 3-D seismic data were used to interpret the location of major stratigraphic markers between wells, and these seismic horizons were used to constrain a time window for a volume-based attribute analysis. Step-wise regression and cross-validation were used to combine seismic attributes to predict porosity in wells where the porosity was known from the well logs. The results of a linear regression porosity model show good correlation ($r=0.74$) between 7 seismic attributes and the observed porosity logs at 11 wells in the study area, but the porosity volume created from the regression model did not display the known geologic features. A probabilistic neural network (PNN) was then trained to look for a non-linear relationship between the input data (the 7 attributes) and the observed porosity at the 11 wells. The correlation was better ($r=0.82$), but the biggest improvement over the linear regression model came in the more geologically realistic predicted porosity distribution.

INTRODUCTION

Prediction of subsurface physical properties is a fundamental problem confronting geologists and geophysicists. This paper tests two different means of predicting porosity between well locations using seismic attributes. Seismic attributes have been used to predict reservoir properties with success (e.g. Russell et al., 1997; Schuelke and Quirein, 1998; Pearson and Hart, 1999; Hart and Balch, 2000), but recently neural networks have been suggested by geophysicists as a means to increase the certainty of the predictions over standard linear regression methods (Ronen et al., 1994; Schuelke et al., 1998).

A concern among geologists is that multiattribute studies may show statistical significance between the attributes and a physical property, but there may be no theoretical basis for using the attributes, and a resulting model may be geologically unrealistic. Following the work of others (Ronen et al., 1994; Kalkomey, 1997; Hirsche et al., 1997; Hart, 1999; Pearson and Hart, 1999), we emphasize the need for the results of an attribute-based prediction to be geologically plausible (in addition to other criteria; see below) before it is accepted. In this paper we use log and seismic data to investigate the geology of the lower Brushy Canyon in the study area. We then employ two different techniques, standard linear regression and a probabilistic neural network (PNN) to generate porosity distribution models of the lower Brushy Canyon from seismic attributes. By comparing the results of the two methods with the geology, we conclude that the neural network provided a better image of the subsurface porosity distribution. This is because the neural network architecture is better able to capture the non-linear relationship between seismic attributes and log-based physical properties. As of the date of completion of this paper, no previous work has been done using neural networks to

predict physical rock properties with an intent to conform strictly to pre-existing geologic knowledge.

GEOLOGIC SETTING

The Delaware Basin is the westernmost basin in the Permian Basin complex of western Texas and southeastern New Mexico. The basin is bound by the Central Basin Platform to the East, The Northwestern Shelf to the North, and the Diablo Platform to the West (Fig. 1). During relative lowstands of sea level in the Permian, siliciclastic sediments bypassed the shelf and were deposited in the basin (Sageman et al., 1998; Montgomery et al., 1999). The Delaware Mountain Group, which consists of the Bell Canyon, Cherry Canyon and Brushy Canyon Formations in descending order, is an example of this kind of sedimentation.

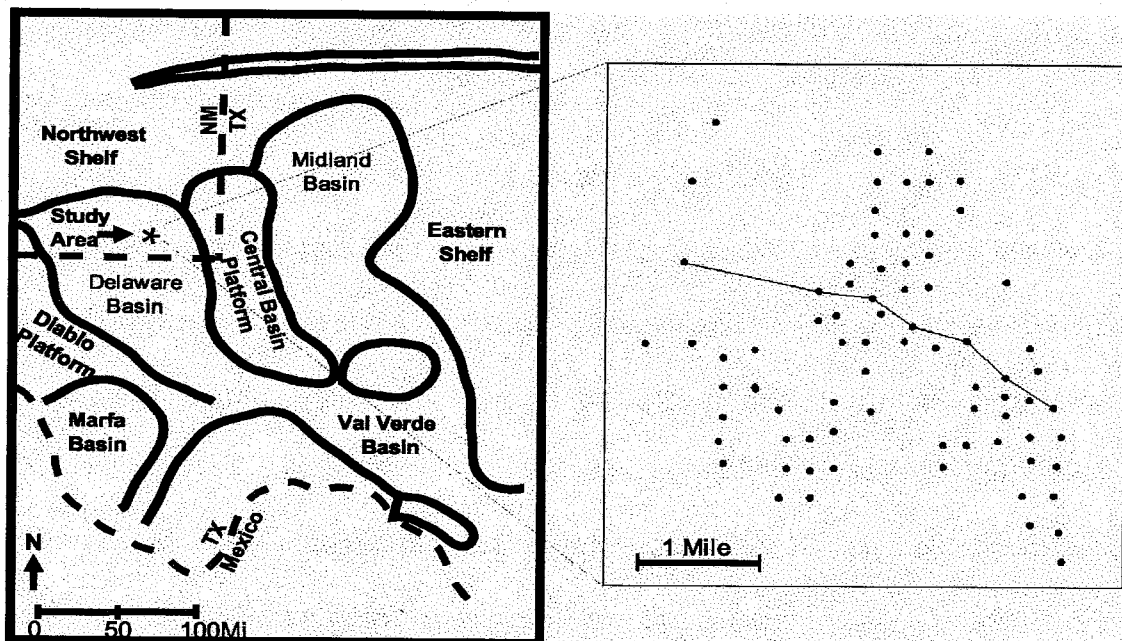


Figure 1: Regional paleogeographic map showing the Permian Basin complex. Approximate location of the study area is noted by the star. After Yang and Dorobek (1995). Also shown is the 16 square mile study area, the locations of the 77 wells, and the location of the cross-section in Figure 3.

The Brushy Canyon Formation includes three major facies: (1) submarine canyon fills in the underlying Victorio Peak Formation, (2) slope deposits consisting of thick successions of interbedded sandstones and siltstones, and (3) basin-floor deposits (Harms and Brady, 1996). Brushy Canyon deposition was due to some gravity flow mechanism, such as either turbidity currents or saline density currents. In addition, Brushy Canyon channel features have previously been mapped extending 50 miles onto the basin floor (Basham, 1996; Montgomery et al., 1999).

The Brushy Canyon Formation consists of up to 1800 feet of interbedded fine-grained sandstones and siltstones, and is informally subdivided into a lower, middle, and upper part. Each of these parts are separated by laterally continuous organic-rich siltstone marker beds that may be tracked throughout the basin using well log information. The lowermost Brushy Canyon is on average about 325 feet thick and thickens basinward. It is interpreted as a system of sand-filled feeder channels and associated fans (Sageman et al., 1998).

MATERIALS AND METHODS

Our database consisted of a time-migrated 3-D seismic survey, wireline logs from 77 wells in and around the study area, and production data. The seismic data cover an area of about 16 square miles (41.4 square km) with a bin size of 110 feet by 110 feet (33.5 m by 33.5 m) and a 3 second two-way travel time (TWT) record length. The 3-D grid is laid out with crosslines oriented approximately north - south and inlines running west - east perpendicular to the crosslines. The seismic data originally consisted of two volumes that were processed into a single volume prior to our interpretation. No information regarding processing was available to us.

We analyzed digital logs for 77 wells for lithology determination and stratigraphic correlation. The main logs used in this study were gamma ray (GR), photoelectric factor (PEF), deep resistivity, and density logs. Sonic logs were available for 21 wells and were used to generate the synthetic seismograms, which were then used to tie the well logs to the seismic data (See Appendix 1). The neutron porosity log was used in the multiattribute study as the target log. A good correlation ($r=0.91$) was found between neutron porosity and sonic velocity assuring us that neutron porosity is dependant upon rock physical properties and not biased towards lithology. Because there are no true shales in the lower Brushy Canyon in this area, there is no reason for overly optimistic neutron porosity values (Justman, in press).

Where possible, log-based stratigraphic horizons were auto-tracked through the seismic data then smoothed. These seismic horizons were then used to constrain the time window for the volume-based attribute study (e.g. Russell et al., 1997). This method was preferred over the horizon-based approach because of the geologic complexity and thickness of the lower Brushy Canyon. Attributes were extracted from the seismic data and ranked by step-wise regression, and the results were tested by validation (Schuelke et al., 1998). We used both standard linear regression techniques and a probabilistic neural network (PNN) to create two predicted porosity volumes for the entire lower Brushy Canyon Formation in the study area. These two models were then evaluated by their ability to predict porosity and image stratigraphic features interpreted from the well logs.

Details of the mathematical basis for these two techniques are provided below. For additional details on the PNN see Appendix 2. Although we had access to a multi-

layered feed-forward neural network (MLFN) architecture, we did not use this method because of its "black box" character (Hampson et al., in press).

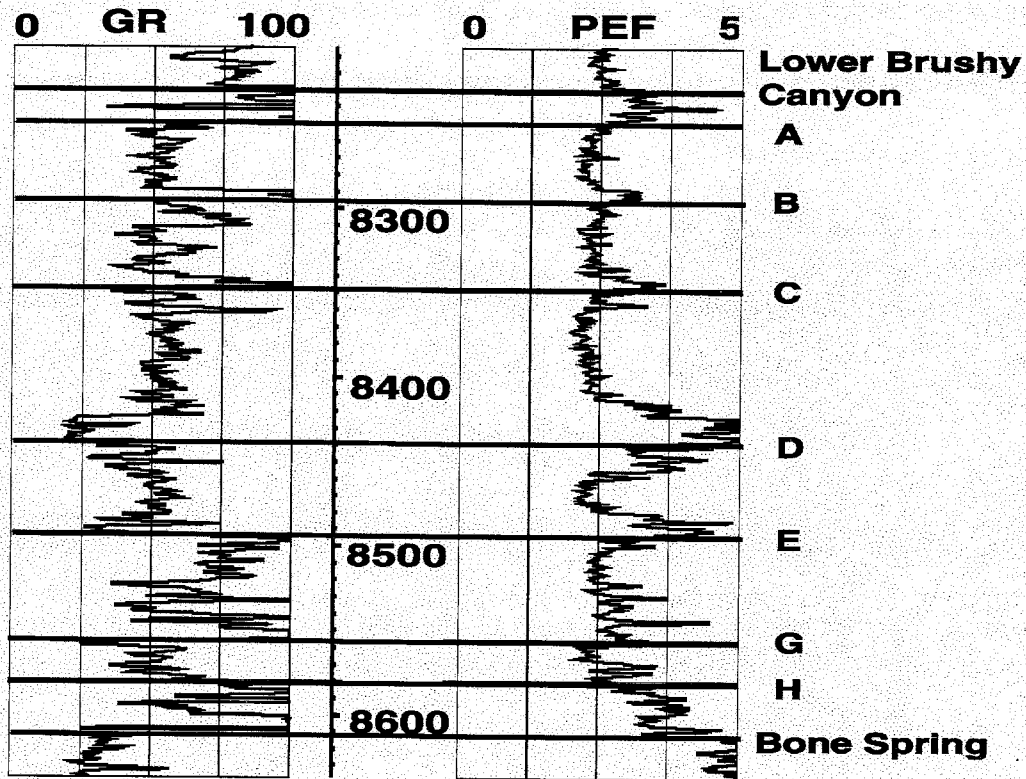


Figure 2: Sample log through the lower Brushy Canyon in this study area. The logs from left to right are the gamma ray (GR), and the photoelectric factor (PEF) logs. Note the relatively thin organic siltstone and limestone layers that separate each of the stratigraphic units. These interbeds are expressed either as abrupt increases in radioactivity as shown in the GR curve (organic siltstones) or zones of low GR values accompanied by high PEF values (limestones).

STRATIGRAPHY

Lower Brushy Canyon Picks

We divided the basal Brushy Canyon Formation into 8 stratigraphic units based on gamma ray (GR), photoelectric factor (PEF), deep resistivity, and density log characteristics (Fig. 2). The units are named alphabetically A through H in descending

order, and are each separated vertically by organic siltstone and carbonate interbeds of varying thickness (generally less than 30 feet). Each of these stratigraphic units have unique well log signatures that could be correlated and tracked throughout the study area with confidence (Fig. 3). For details on stratigraphic interpretations, see Appendix 1.

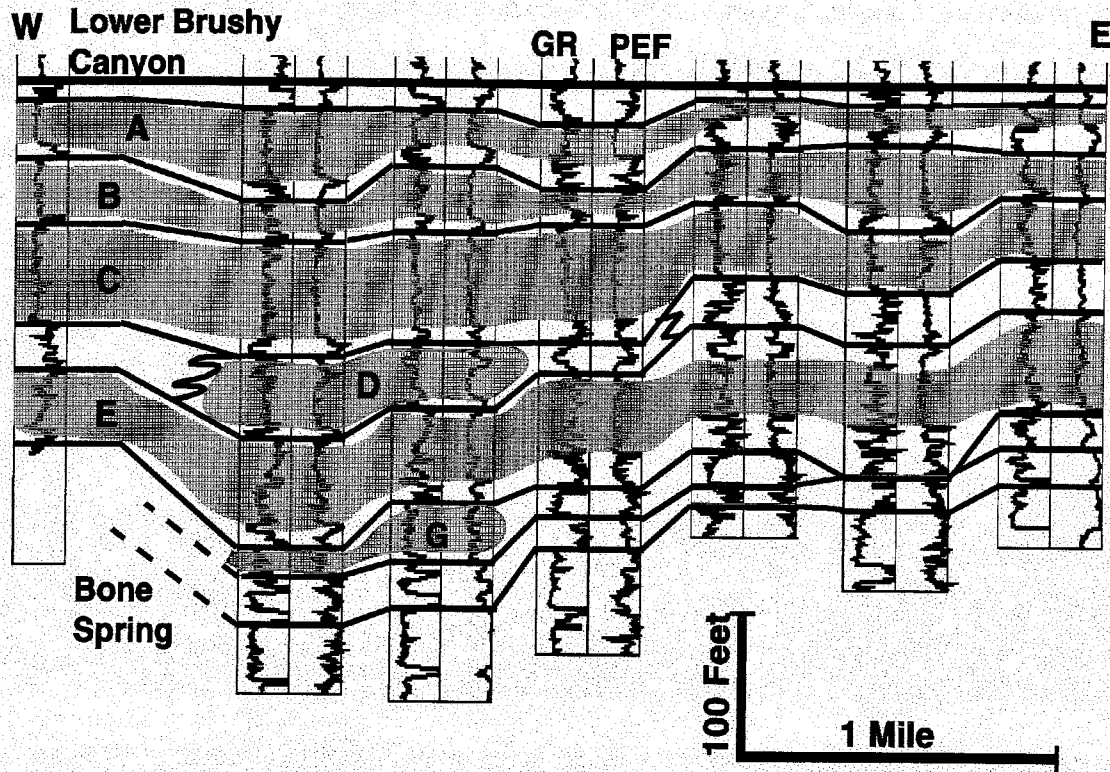


Figure 3: NW-SE stratigraphic cross-section through the study area datumed at the lower Brushy Canyon. The location of the cross-section is shown in Figure 1. The logs used are the GR (left) and the PEF (right). The shaded regions denote the significant sandstone bodies in the lower Brushy Canyon in this study area, and the letters within the shaded regions correspond to the individual stratigraphic units.

Unit A is the top unit stratigraphically. It is about 5 to 20 feet below the top of the lower Brushy Canyon pick. In the central and western parts of the study area, Unit A is a massive sandstone ranging from 25 to 55 feet thick (Fig. 4A). In the eastern part, it is

characterized by a coarsening upwards package that is considerably less thick (less than 20 feet).

Unit B is also a massive sandstone (40 to 65 feet thick; Fig. 4B) in the central and western region, and a coarsening upwards sequence in the southeast (30 to 45 feet thick).

The thickest and cleanest sandstone in the lower Brushy Canyon Formation in this area is Unit C. It ranges from 35 to 100 feet thick (Fig. 4C) and is almost everywhere composed of 95 to 100 percent sand. Slightly higher siltstone contents may be found in the extreme northwest and southeast regions.

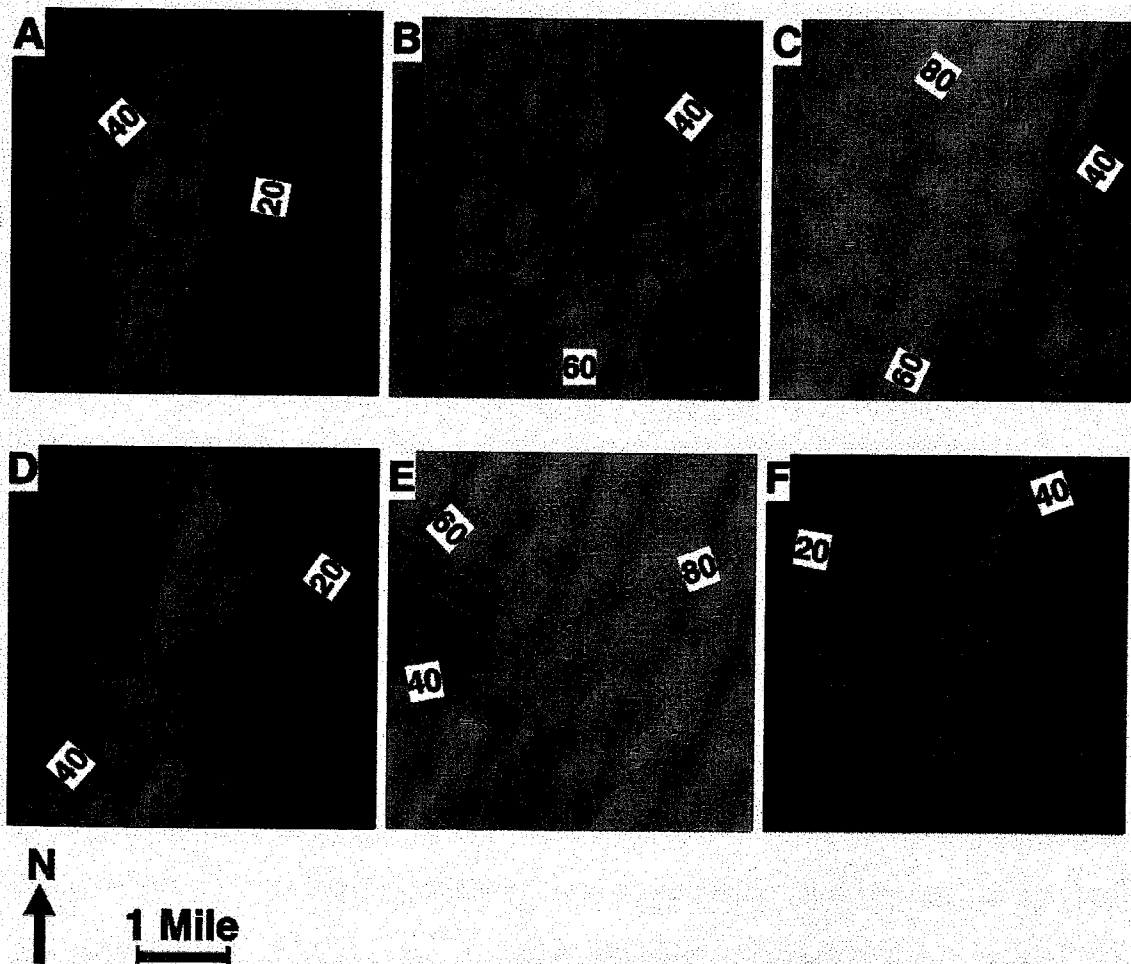


Figure 4: Isopach maps for each of the units in the lower Brushy Canyon Formation. The contour interval is 10 feet with yellow tones denoting thicker zones. The scale and color scheme are the same for each map.

Units D and F are laterally equivalent units. Unit D consists primarily of sandstone with some limestone interbedding to the east, and it is only present in a NNE - SSW strip more than a mile wide in the middle of the study area (Fig. 4D). Unit F is a package of approximately equal thickness that consists of organic siltstones with dolomite interbeds. It is located on both the northwest and the southeast sides of Unit D.

Unit E is a heterolithic unit which made details of internal correlations problematic. This unit is comprised of a massive sandstone in the northwest, a fining upwards to coarsening upwards package in the center region, and a slightly more carbonate unit in the southeast. The thickest (70 to over 100 feet) area is in the eastern to southeastern regions where the unit is characterized by a higher siltstone content (Fig. 4E).

Below Unit E is Unit G. The thickest sandstones of this interval strike NNE - SSW (Fig. 4F). To the southeast of this linear feature, Unit G primarily consists of a limestone with little if any sandstone interbedding (generally less than 5 feet).

Unit H may be considered as a transitional unit from the underlying Bone Spring Formation to the sandstone units of the basal Brushy Canyon. It is chiefly a dolomitic limestone with varying siltstone content and negligible sandstone.

Seismic Horizons

Figure 5 shows a west - east transect through the center of the 3-D seismic data volume. Once the wells were accurately tied to the seismic data by way of synthetic seismograms, it was then possible to interpret horizons of interest in the seismic data. The top of the lower Brushy Canyon is characterized by a peak that may be tracked

throughout the entire data set. The top of Unit C almost everywhere corresponds to the trough directly below the lower Brushy Canyon reflector. Because of the thickness and relatively low velocity of Unit C, it can accurately be tracked throughout most of the data set as a high amplitude trough. At most locations within this study area, the other stratigraphic units are below vertical seismic resolution due to the thinness of the bed and the relatively low acoustic impedance contrast with adjacent units. For details on seismic interpretations, see Appendix 1.

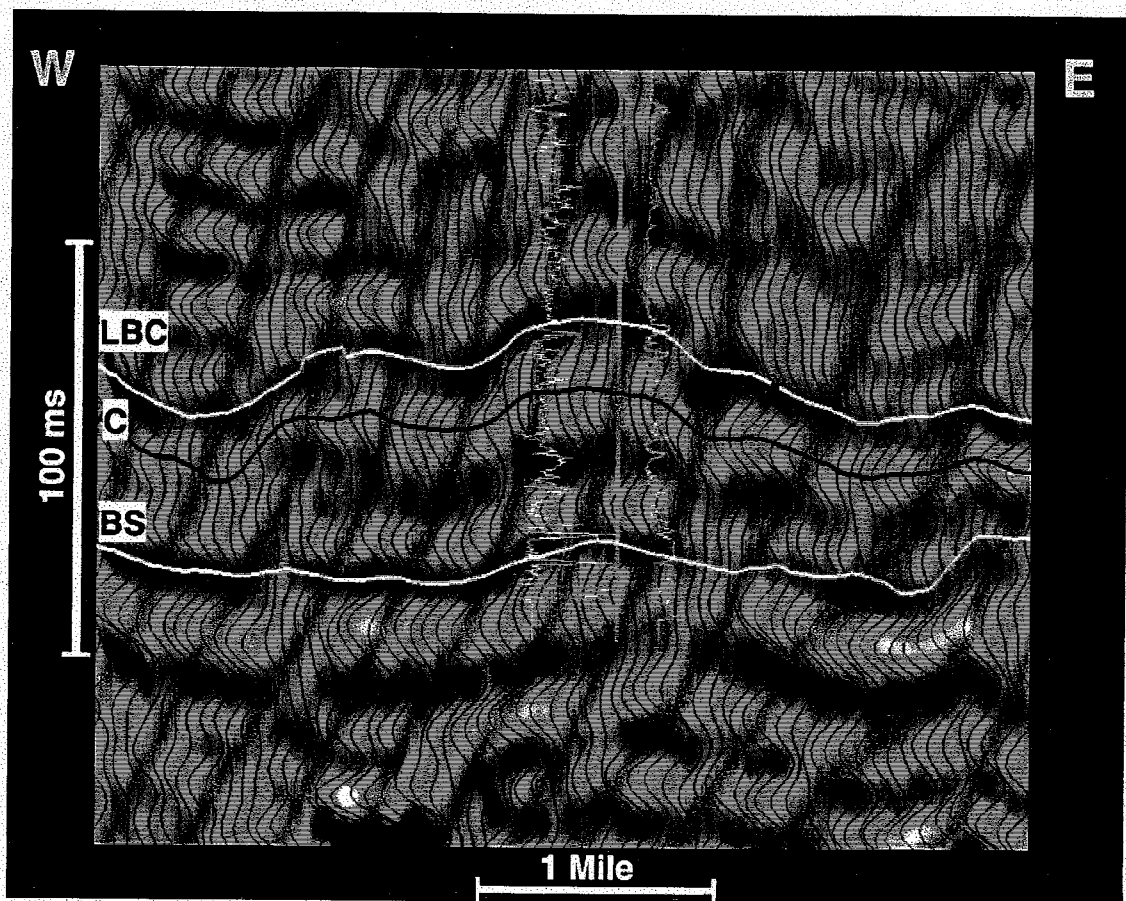


Figure 5: West - east seismic transect near the center of the study area. The lower Brushy Canyon (LBC - white) is shown as a peak at about 1200 ms (TWT). Unit C (C - black) is characterized by a high amplitude trough at about 1220 ms (TWT). The Bone Spring Formation (BS - white) is shown as a discontinuous peak at about 1250 ms (TWT). The wireline logs shown are the GR (left) and the PEF (right).

At other locations within the Delaware Basin, the Bone Spring Formation is characterized by a high amplitude peak because of a relatively abrupt transition from the basal Brushy Canyon sandstones into the high-velocity Bone Spring carbonates (Hardage et al., 1998; Hart, 1998). However, in our study area, the Bone Spring is overlain by up to 80 feet of high-velocity sandstones and carbonates (Unit H and the eastern region of Unit G). In this case, the top of the Bone Spring corresponds to a peak although locally a phase reversal is present where thick carbonates overlie the Bone Spring.

Discussion - Stratigraphy

The lower Brushy Canyon Formation is thought to be made up of a system of channels that transported sandy sediment to the basin floor (Basham, 1996; Sageman et al., 1998; Montgomery et al., 1999). All of the isopach, gross sand, and percent sand maps, and the cross-sections show strong evidence for channel-like structures trending in the N-S to NE-SW directions (Fig. 4). In places, isopach trends appear to be discontinuous, lacking channel geometry. This could be due to: a.) the contouring algorithm's solution in areas of sparse well control; or b) geologic reasons, such as pre-existing seafloor relief or post-depositional erosion by subsequent flows, that affect the actual thickness of individual sandstone bodies.

A cross-section perpendicular to these channel trends (Fig. 3) shows that the entire basal Brushy Canyon is thickest in the center region and thins to the west and the east. Furthermore, the thickest part of each succession is located in the center of the study area with each unit becoming thinner and less sandy away from the channels. This suggests that the sediment source location and transport axes did not change significantly during the deposition of the lower Brushy Canyon in this region as there is very little

lateral shift from one channel to the next. The only exception is the addition of a new sediment source to the Northeast during the deposition of Unit B (Fig. 4B).

The structure at the top of the underlying Bone Spring Formation appears to be the primary determining feature for the channel locations (Fig. 6). Bone Spring topography is thought to have controlled basal Brushy Canyon channel locations at other areas in the Delaware Basin (Thomerson and Catalano, 1996). At this level, the study area is characterized by a prominent structural high just southeast of center. Each of the subsequent channels filled in the structural lows of the underlying unit.

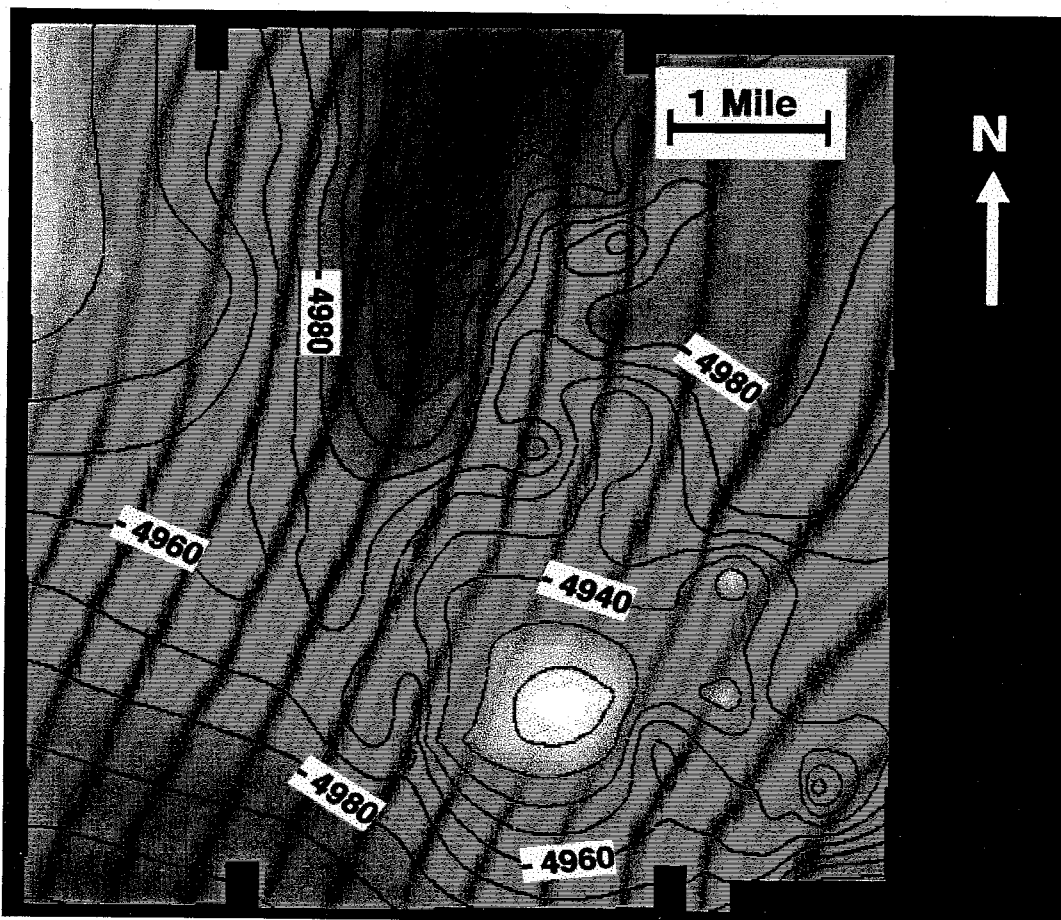


Figure 6: Depth-converted structure map of the top of the Bone Spring Formation calculated from the seismic data. The contour interval is 10 feet, and the color scheme is such that lighter tones depict structural highs. Note the north - south trending valley in the center of the study area. This valley was the pathway for the Unit G channel, and subsequent channeling was likewise controlled by underlying structure.

The isopach maps in Figure 4 show evidence of channel sediments overflowing and spilling over the sides of the channel. This depositional pattern has been noted elsewhere in the subsurface as well as in outcrop (Basham, 1996; Gardner and Sonnenfield, 1996). The sandstone of Unit D is bordered on both sides of the channel by the stratigraphically equivalent siltstones and dolomites of Unit F (Fig. 4D). It is possible that the channel cut into the underlying sediments of Unit F, and as sand filled the channel, it began to spill over the sides.

Vertical stacking and siltstone capping of channels is typical of low-stand fan deposition. Successive density currents may take similar paths, each depositing a broad, lenticular layer of sand overlain by a silty layer (Bouma, 1996). As a result, the lower Brushy Canyon consists of a vertical succession of channeled sandstones each separated by a laterally extensive siltstone or carbonate layer.

SEISMIC ATTRIBUTE STUDY

Methods

Having established a stratigraphic framework for the basal Brushy Canyon in this study area, we sought a relationship between log-derived physical properties and seismic attributes. Quite simply, a seismic attribute is a derivative of a basic seismic measurement which may be extracted along a horizon or summed over a time window (Brown, 1996). There are several factors that go into seismic multiattribute analyses, such as whether to perform a horizon- or a volume-based analysis, which attributes to use, the weight assigned to each attribute in the final equation, and the number of attributes to use.

For an attribute study to be judged successful, several criteria need to be met. These are: a) the results must be statistically significant, b) a known or suspected relationship between the attribute and physical properties must exist, c) the results must be geologically plausible, and d) the results must agree with available engineering data.

We chose a volume-based approach due to the thickness and complexity of the lower Brushy Canyon stratigraphy, and its effect on internal reflections in the seismic data. The time window from the top of the Lower Brushy Canyon Formation to the Bone Spring was chosen as the window of interest for seismic attribute extraction and all seismic-guided interpretations. For details on attribute-based analyses, see Appendix 1.

The choice of which attributes to extract was defined by the capabilities of the software. We ranked the attributes according to their correlation to the neutron porosity, and weighted appropriately, by step-wise regression following the methods of Hampson et al. (in press).

The number of attributes used in this study was determined by cross-validation. In this approach, wells are excluded one at a time while the remaining wells are used to predict the excluded one. This technique seeks to eliminate the problem of over-fitting the data associated with using too many attributes (Schuelke, et al., 1998), a problem recognized by Kalkomey (1997). The point at which the addition of a new attribute increases the validation error and becomes too well-specific is the cutoff for the optimal number of attributes to be used. Based on these results, a linear regression model was used to create a predicted porosity volume over the time window of interest.

A probabilistic neural network (PNN) was then trained to predict porosity over the same volume. Again, by performing the step-wise regression and validation tests

before training the neural network, we eliminate the problem of over-fitting the data (Schuelke et al., 1998). Ronen et al., (1994) pointed out that it may be important to look for non-linear relationships between seismic attributes and rock properties. Artificial neural networks (ANNs) can be trained to determine those non-linear relationships.

We then compared the porosity volumes created from both the standard linear regression model and the PNN model. The models were evaluated as to their statistical significance and their ability to create a porosity volume that conformed to the log-based geologic interpretations.

Results - Attribute Study

We extracted 19 attributes from the seismic volume, then narrowed that list down to seven based on analysis of the validation error. These attributes are given in Table 1 along with associated application error (the average error using 11 wells with neutron porosity logs that could be accurately tied to the seismic data) and validation error (the average error leaving one well out at a time). The attributes are:

| <u>Seismic Attribute</u> | <u>Application Error (%porosity)</u> | <u>Validation Error (%porosity)</u> |
|-------------------------------------|--|---|
| 1.) Smoothed Inversion ² | 2.64 | 2.76 |
| 2.) Integrated Absolute Amplitude | 2.54 | 2.74 |
| 3.) Amplitude Weighted Phase | 2.45 | 2.71 |
| 4.) Average Frequency | 2.36 | 2.62 |
| 5.) Instantaneous Phase | 2.31 | 2.61 |
| 6.) SQRT(Minimum Continuity) | 2.25 | 2.59 |
| 7.) Derivative | 2.20 | 2.58 |
| 8.) Amplitude Weighted Cosine Phase | 2.12 | 2.62 |

Table 1: List of the seismic attributes chosen and ranked by step-wise regression and the associated application error (includes all 11 wells) and validation error (excludes one well at a time as the target well). The errors are average distances between the predicted porosity at each sample and a Y=X line.

1. The Smoothed Inversion is a 50 ms smoothed rendering of the seismic inversion constrained by the lower Brushy Canyon and Bone Spring horizons. The inversion is an estimate of the seismic acoustic impedance based on the well data and the seismic wavelet. Because this inversion is based on well data, it is not a true seismic attribute. Accordingly, the inversion result should be smoothed to where the well uniqueness is lost. The smoothed result keeps the low-frequency component, or trend, making it useful for predicting rock properties. Since acoustic impedance and porosity are generally inversely related, the smoothed inversion proved to be a good starting point for porosity prediction.
2. The Integrated Absolute Amplitude is the running sum of the reflection strength minus a smoothed version of the reflection strength. This attribute enhances strong amplitudes, whether positive or negative, which denote high acoustic impedance contrasts which may be indicative of stratigraphic or facies changes.
3. Amplitude Weighted Phase is the product of the reflection strength and the instantaneous phase.
4. Average Frequency is a running average of the instantaneous frequency. The average instantaneous frequency tracks dominant frequency characteristics that may be associated with changing lithology or stratigraphy.

5. Instantaneous Phase is independent of the reflection strength, and thus emphasizes weak coherent events. In stressing the continuity of events, it can be useful in locating stratigraphic pinchouts and channel features.
6. Minimum Continuity, or coherency, is a measure of the lowest similarity from one seismic trace to a neighboring trace over a time window. The results show abrupt contrasts in impedance due to stratigraphic or facies changes. Volumes of coherency data may be used to locate channel edges due to the variance in reflection character at the channel margins (Bahorich and Farmer, 1995).
7. The Derivative is the difference between the seismic trace amplitudes of one sample and the preceding sample. This emphasizes abrupt impedance contrasts that may be due to stratigraphic or facies changes.

$$\Phi(t) = w_0 + A_1 w_1(t) + A_2 w_2 + A_3 w_3 + A_4 w_4 + A_5 w_5 + A_6 w_6 + A_7 w_7 \quad (1)$$

The results of the linear regression multiattribute analysis are shown in Figure 7, and a cross-plot of the data is shown in Figure 8. The results were obtained using equation (1), where Φ is porosity, A_n is the attribute, w_n is the weight applied to the attribute, and t is time (Russell et al., 1997). The correlation coefficient for the linear regression model is $r=0.74$ with an average error of 2.2% (porosity units). The validation testing yielded a correlation coefficient of $r=0.63$ with an error of 2.6% (porosity units). The regression method modeled the trends of the porosity curve, but it failed to accurately pick up the extreme values in the curve. Figure 8 shows that the model over-predicts the lower porosity values and under-predicts the higher values. The end model

would thus be a smoothed version of the porosity curve, but the trends of high and low porosity should be adequately predicted.

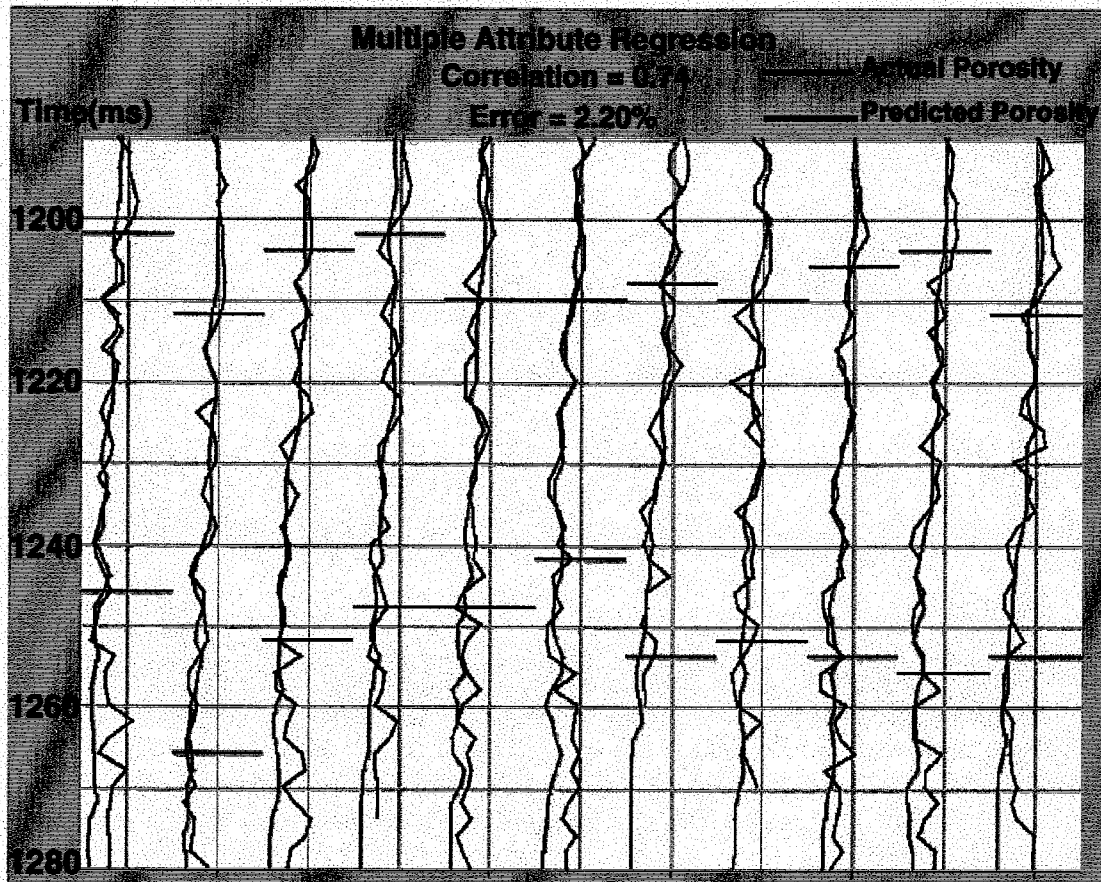


Figure 7: Application of the linear regression method to predicting porosity. The blue horizontal lines at each well depict the time window from the lower Brushy Canyon to the Bone Spring. Note that the model (red) adequately predicts the trends in the actual porosity curve (black), but fails to pick up the extreme porosity values. The correlation is only valid within the indicated time window.

Training the PNN provided better results ($r=0.82$ with an average error of 1.9% (porosity units)). However, the validation error remained the same ($r=0.62$ with an error of 2.6% (porosity units)). These results were obtained using the following equation:

$$L' = \frac{\sum_{i=1}^n L_i \exp(-D(x, x_i))}{\sum_{i=1}^n \exp(-D(x, x_i))} \quad (2)$$

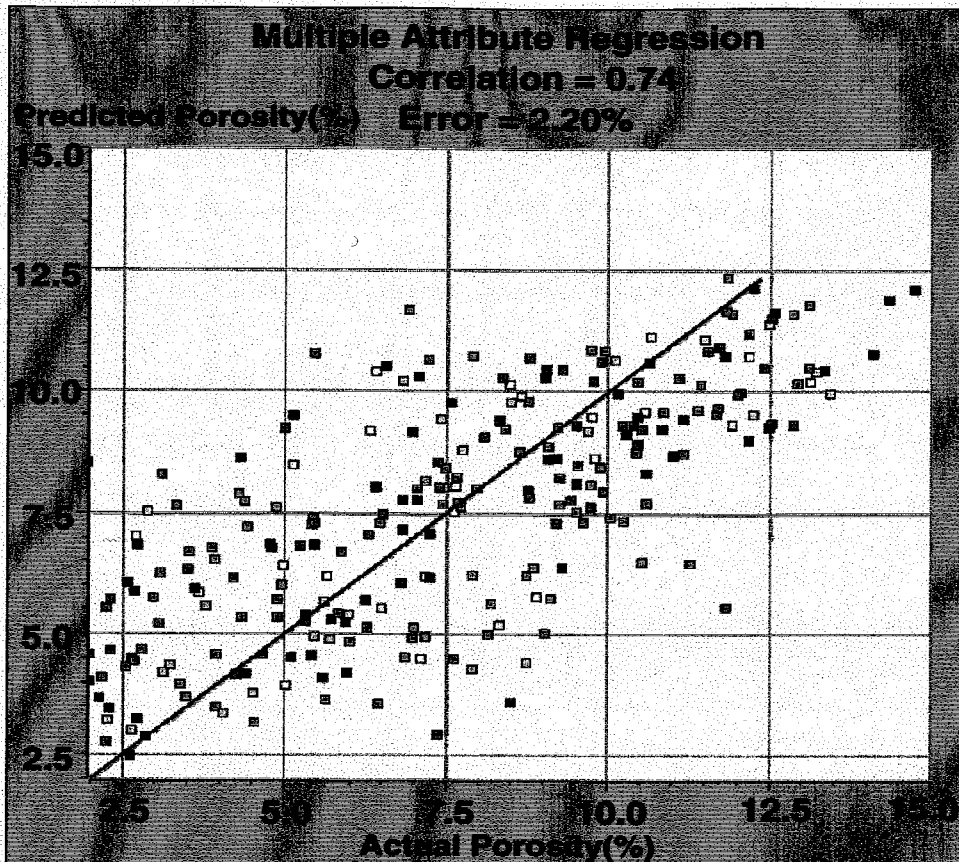


Figure 8: Cross-plot of the linear regression model results. Each data point represents a different well. The red line is a $Y=X$ line. Note the tendency to over-predict the lower actual porosities and to under-predict the higher porosity values.

where L' is the predicted porosity value at each sample, L_i is the actual porosity value, and $D(x, x_i)$ is the distance between the input point and each of the training points (Masters, 1995; Hampson et al., in press). For details on the procedures and the methodology of the PNN, see Appendix 2 at the end of the paper. The PNN results are shown in Figure 9, and a cross-plot of the data is shown in Figure 10. Figure 9 shows that the PNN is not only predicting the trends in the porosity curves, but it is also better predicting the extreme values. The cross-plot still reveals the tendency to smooth the porosity curve, but now we expect to see greater detail in maps generated from this model over the linear-regression model.

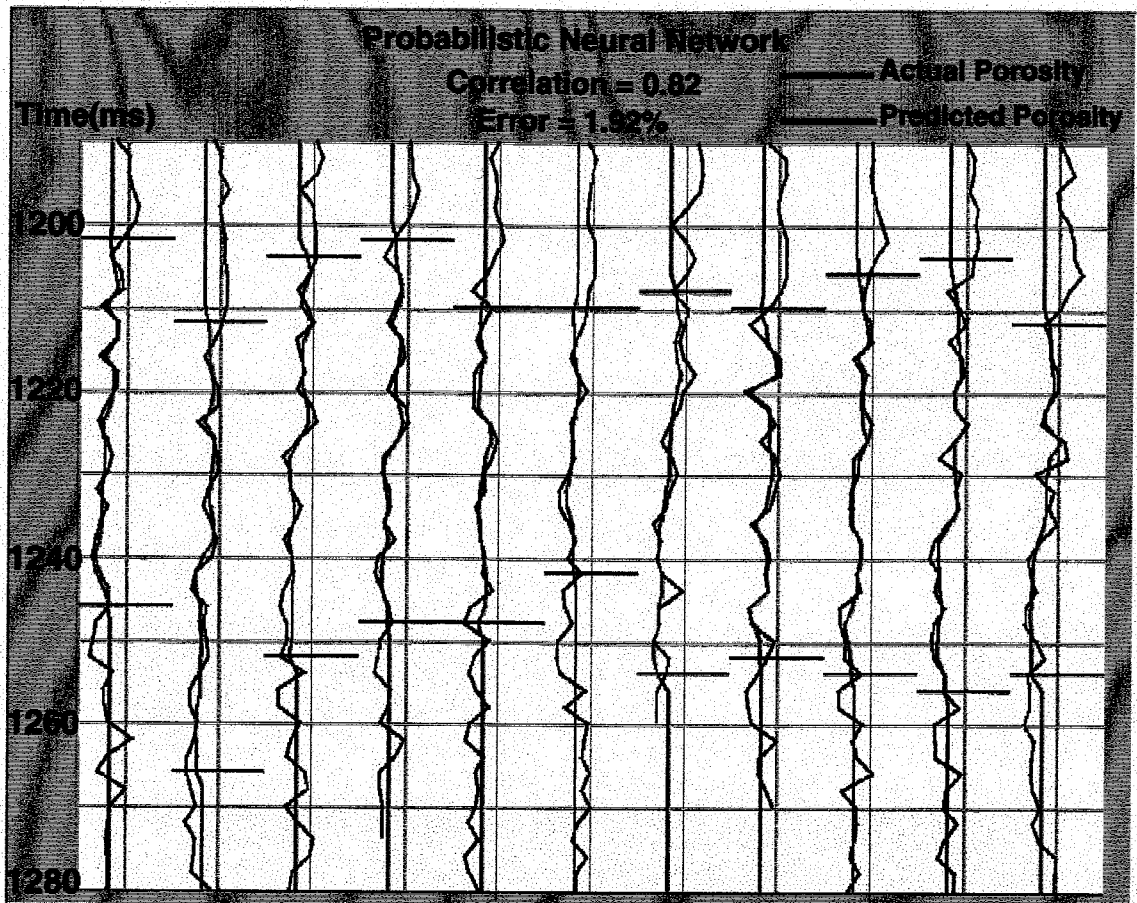


Figure 9: Application of the probabilistic neural network to predicting porosity. As in Figure 7, the blue horizontal lines depict the time window. The PNN modeled porosity curve (red) more accurately predicts the actual porosity curve (black) than the standard linear regression model. The PNN also appears to have predicted the extreme porosity values. The correlation is only valid within the indicated time window.

Figure 11 is a smoothed average predicted porosity map of Unit C based on the linear regression model. Some high porosity north - south striking linear features appear in the southwestern portion of the study area, but they die out to the North. The orientation of the nine wells in the center of the study area is approximately parallel to the channel of Unit C (Fig. 4C). The two wells in the southeaster corner are located outside the channel.

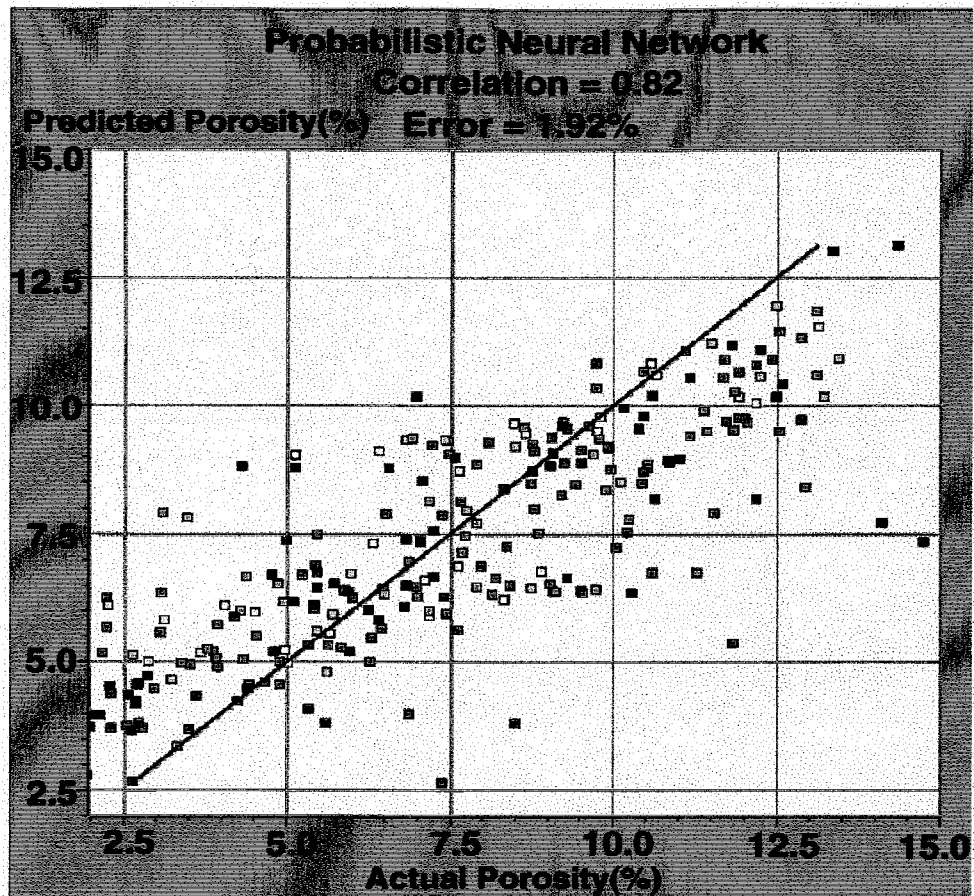


Figure 10: Cross-plot of the PNN results. Each data point color represents a different well. As in Figure 8, the model tends to over-predict the low porosities and under-predict the high porosities, but the PNN data points are arranged noticeably closer to the Y=X line.

To enhance the linear features, because of the vertical stacking of the channels as seen in Figure 4, we created an average predicted porosity map of units A through D (Fig. 12). As expected, the north - south linear features are enhanced because of the greater time window, but the high porosity zones still appear to die out to the North. The edge of the high porosity zone trends north - south just east of the wells in the center of the study area. However, the porosity seems to be randomly dispersed in the western region.

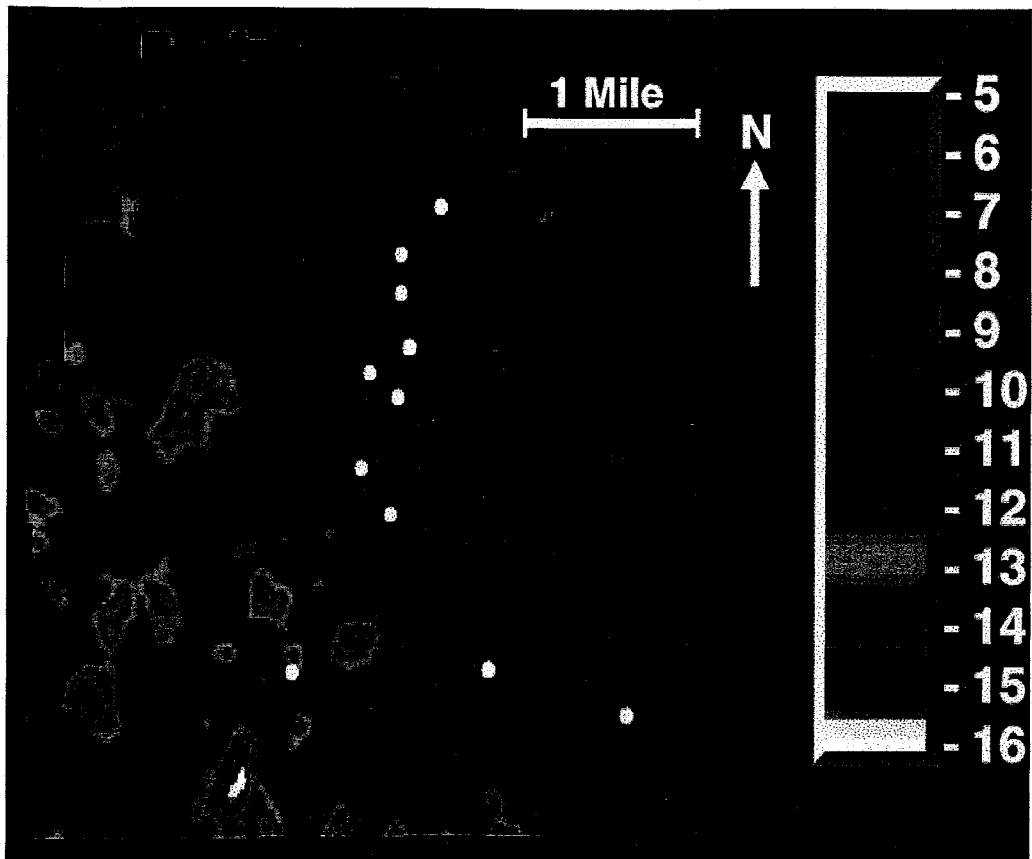


Figure 11: Linear regression predicted porosity map of the entire Unit C interval. Linear trends of high porosity in the northeast - southwest direction occur in the Southwest, but die out to the North.

Another map of the average predicted porosity of Unit C was created using the PNN model (Fig. 13). In addition to the more distinct north - south linear feature that runs through the center of the study area, the porosity distribution is more uniform in the southern and northern halves than in the linear regression model (Fig. 11).

The PNN result was then used to create an average predicted porosity map of units A through D (Fig. 14). As was the case in Figure 13, the neural network model displays more evenly distributed porosity values than the linear regression model. The

edges of the high porosity zone that runs north - south through the center of the study area are much more distinct than the those the linear regression result predicted (Fig. 12).

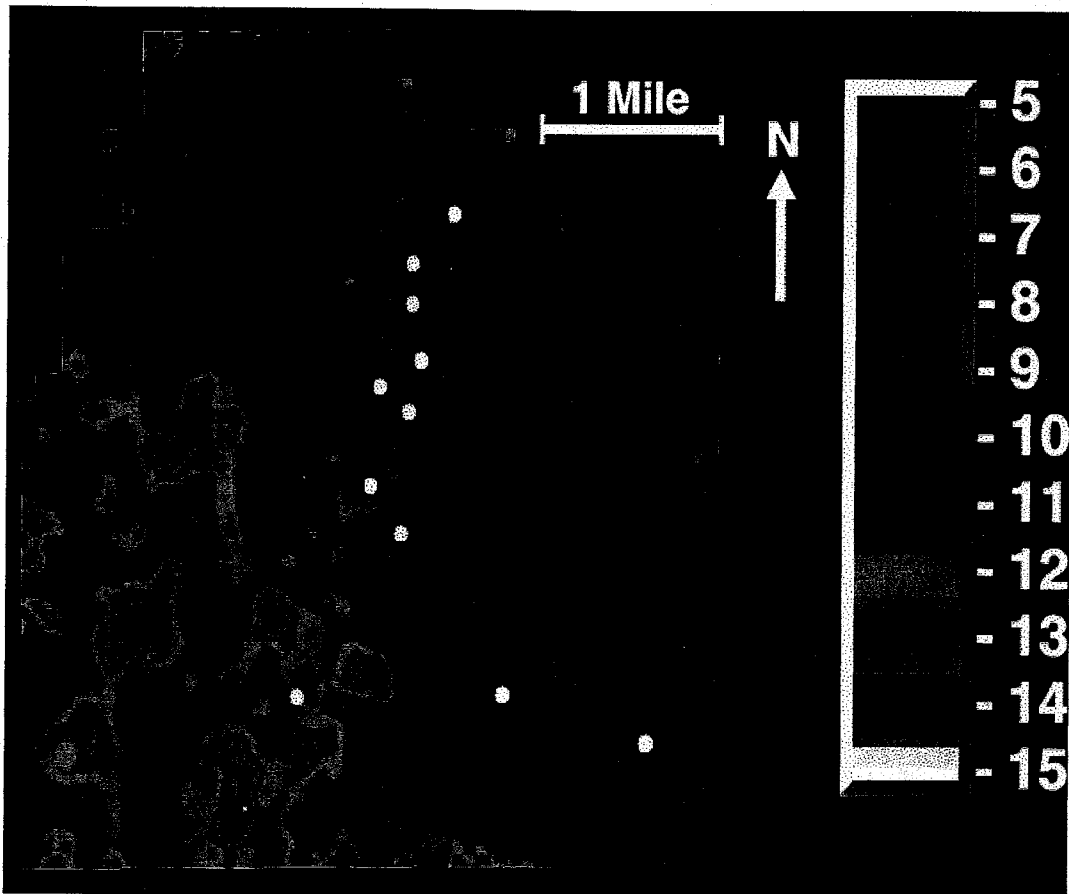


Figure 12: Linear regression predicted porosity map of units A through D interval. Due to the increased time window and the vertical stacking of channels in units A through D, channel features are now enhanced, but the high porosity trends still die out to the North in areas of greater well control.

Figure 15 shows an isopach map of Unit D (Fig. 4D) compared to the average predicted porosity map of the same unit based on the PNN model. The linear feature in the porosity map is not only identical in orientation to the channel in the isopach map, but also in location. Stratigraphic picks on 77 well logs went into generating the isopach map

on the left, while only 11 wells were used as input in making the porosity map on the right.

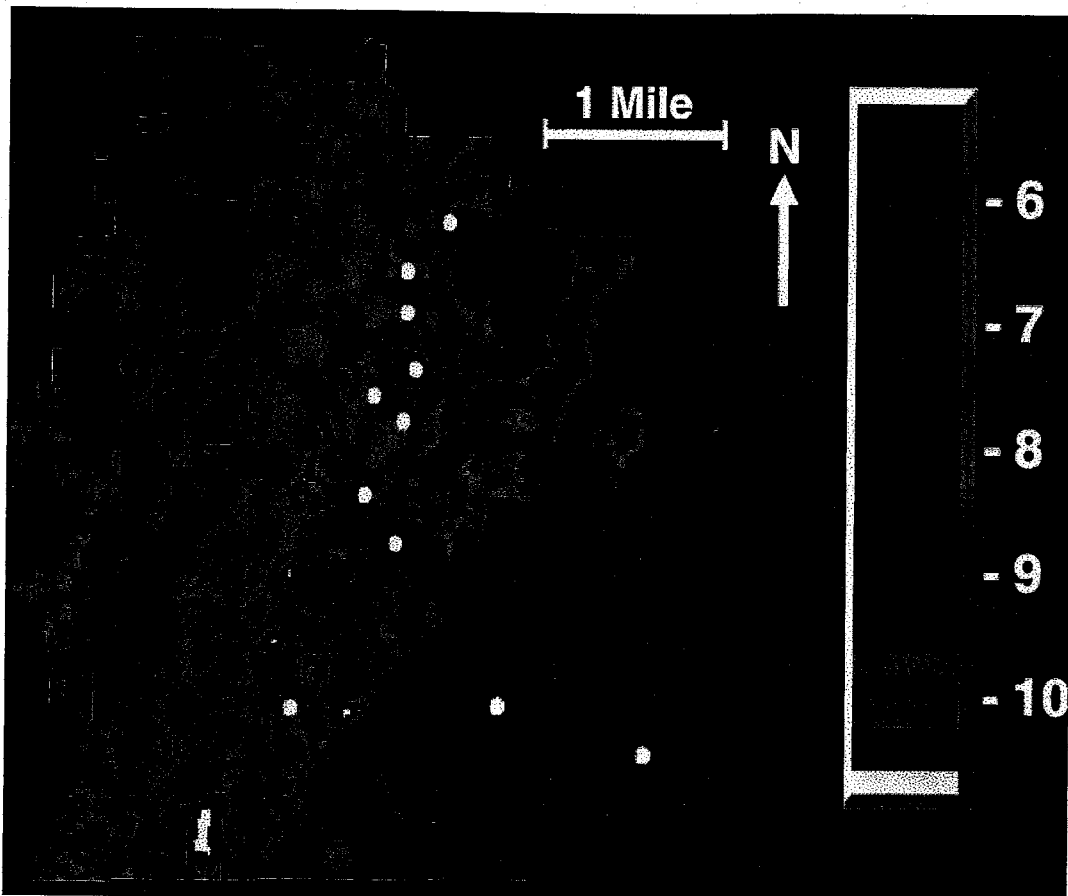


Figure 13: PNN predicted porosity map of the entire Unit C interval. Note that the high porosity zones in the Southwest are diminished from 15-16% (Fig. 11) to 10-11%. Other wells in this area show average Unit C porosities to be about 10.2%. The neural network also predicted more uniform porosities throughout the channel, and more precisely modeled the channel margins in the East and the West.

As a final test of the PNN prediction, we tested our results against eight wells (selected because they represent various geographic locations in the study area) that had been excluded from the multiattribute study because they lacked sonic logs. Table 2 shows the actual porosity compared to the predicted average porosity over the Unit C time window using both the linear regression and the PNN models. The PNN predicted

the actual average porosity within 1.4% (porosity units), whereas the regression model predicted the average porosity within 2.2% (porosity units).

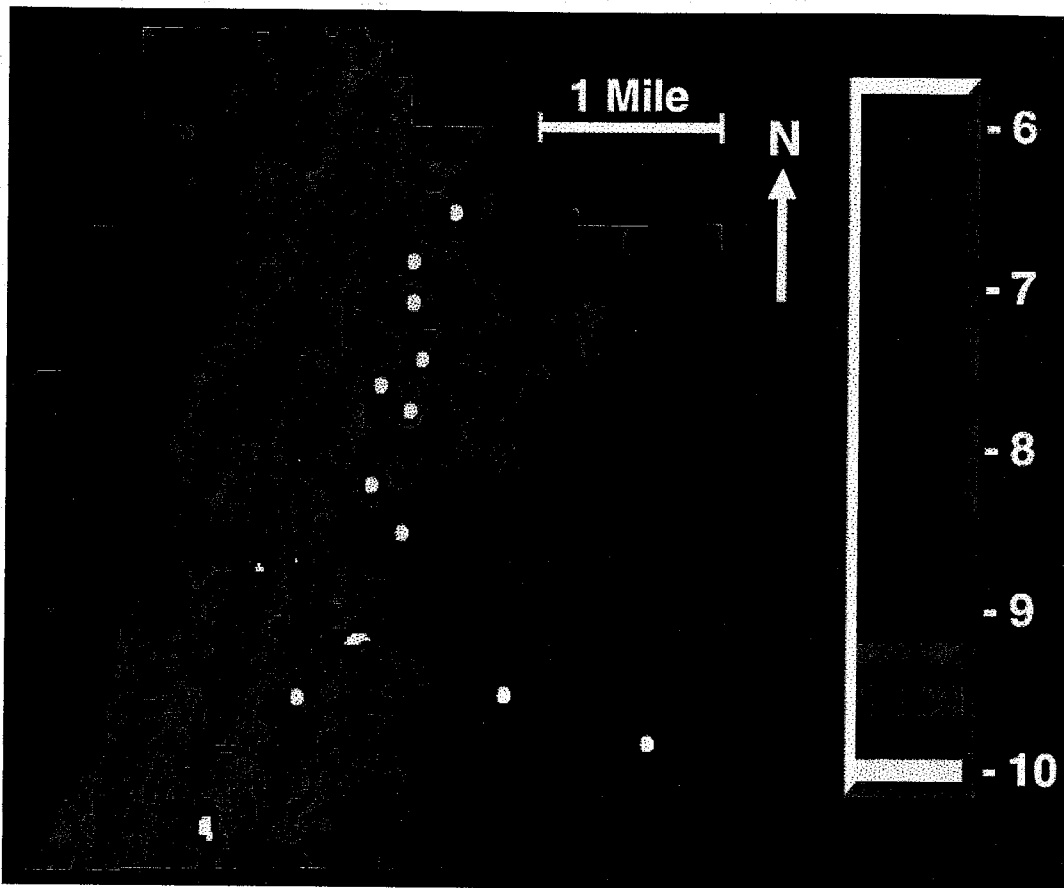


Figure 14: PNN predicted porosity map of stratigraphic units A through D. The channel margins are now more enhanced because of the greater time window. Also, the PNN predicted more uniform porosities over the entire channel volume than the linear regression model (Fig. 12) despite the same sparse well coverage in the Southwest.

Discussion

The exact origin of the porosity in the lower Brushy Canyon is unknown. The most likely explanation is that porosity is a combination of depositional and diagenetic processes, with the diagenetic events destroying primary porosity (Behnken, 1996; Montgomery et al., 1999). Because cleaner sandstones typically have greater original

porosity than poorly sorted sandstones, we would expect to see higher predicted porosity in the high depositional energy channels where percent sand content is higher than outside the channels.



Figure 15: Comparison of the Unit D isopach (Figure 4D) with a contour interval of 10 feet and the smoothed average predicted porosity map of the entire Unit D time window using the PNN model. In addition to capturing the true channel orientation, the predicted channel also appears in the same location as interpreted from the isopach map.

| <u>Approximate Location</u> | <u>Actual Porosity (%)</u> | <u>Regression Error (%)</u> | <u>PNN Error (%)</u> |
|----------------------------------|----------------------------|-----------------------------|----------------------|
| South center main channel | 10.7 | 12.5 | 10.0 |
| West of center of main channel | 11.4 | 12.5 | 10.0 |
| Southwest of channel center | 10.3 | 11.0 | 10.0 |
| Just outside channel to the west | 8.1 | 14.0 | 9.5 |
| Just outside channel to the east | 10.5 | 7.5 | 8.0 |
| Outside channel to the east | 11.7 | 8.5 | 9.0 |
| South of center of main channel | 12.4 | 12.0 | 10.0 |
| Northeast of channel center | 10.0 | 11.5 | 10.0 |
| <u>Average Error</u> | | 2.2 | 1.4 |

Table 2: A list of eight wells not used in the multiattribute study whose average Unit C porosity is known and tested against the predictions of the regression and the PNN models. Approximate locations relative to the channel are given next to the well number. At wells located both inside and outside the channel, the PNN predicted the porosity more accurately than the standard linear regression model.

The most obvious difference between the linear regression porosity maps (Figs. 11 and 12) and the neural network maps (Figs. 13 and 14) is the more even distribution of porosity from the southern to the northern half of the study area in the maps based on the neural network model. The percent sand content maps we generated from log-based lithology interpretations to assist our channel interpretations (not shown) depicted relatively uniform sand distribution throughout the channel, and the percentages diminished with increasing distance from the channel axis. This suggests that porosity should be evenly distributed throughout the channel and decrease with distance away from the channel axis assuming spatially uniform diagenesis. Although maps produced from both models show linear features where channels are seen on the isopach maps (Fig. 4), the PNN porosity maps show a more distinct channel edge on the east and west sides.

Figure 11 shows patches of high porosity (15-16%) in the southwestern part of the study area. The actual average porosity from the well drilled in that region is 10.2%. Similar porosities are recorded in other wells in that area that were not included in the seismic attribute study because they did not have sonic logs (Table 2). A comparison with Figure 13 shows that it also has patches of higher porosity in the same region, but the values are lower (10-11%), and closer to the actual values. Porosity values predicted using the regression model were closer to the actual porosities where there was greater well control than in areas of sparse well coverage. The measured average porosity from a well in this area is 10.5%. The regression model predicted values of 10-12% in this area, which is close to the actual porosity. The PNN model in Figure 13 shows predicted porosities between 9 and 11% consistently throughout the channel. This raises the

question of why the neural network predicted porosity better and more consistently than the linear regression model.

We believe that the neural network predicted the porosity more accurately because the relationship between the seismic data and the well log data was a much more complex one than the linear regression model was predicting. The regression model accurately predicted the porosity in areas of dense well control, but failed where the well control was limited (the Southwest). The PNN was able to successfully determine the non-linear relationship between the seismic data and the well data.

Another way to test the accuracy of the PNN model is to compare the predicted porosity map of a unit to its respective isopach map. Figure 15 shows the Unit D isopach map (left) and the average predicted porosity over the Unit D interval as predicted by the neural network (right). Because the porosity on either side of the Unit D channel is lower than the porosity in the channel, as determined from the well logs, the porosity map should be identical with the isopach map. In addition to the near-perfect channel orientation match, we note that the channel was similar in dimensions and location despite the significant reduction of well control. There is no well control west of the Unit D channel with which to constrain the channel in the PNN model. Based solely on the non-linear relationship between well log data and the seismic attributes, the PNN was able to predict the edge of the high porosity zone at the western channel margin.

Table 2 lists 8 wells scattered throughout the study area where the average porosity of Unit C is known. Wells 4, 5, and 6 were drilled outside of the main Unit C channel where well coverage is minimal. The PNN still predicted the porosity within the validation error, while the regression model greatly over-predicted the low porosity and

under-predicted the higher porosities. The other five wells were drilled inside the main Unit C channel, but mostly away from the dense well coverage in the North. The linear regression technique over-estimated porosity in the southern half of the channel, which is inaccurate in light of the actual uniform (10-12%) channel porosity, whereas the PNN predicted this uniformly distributed porosity trend.

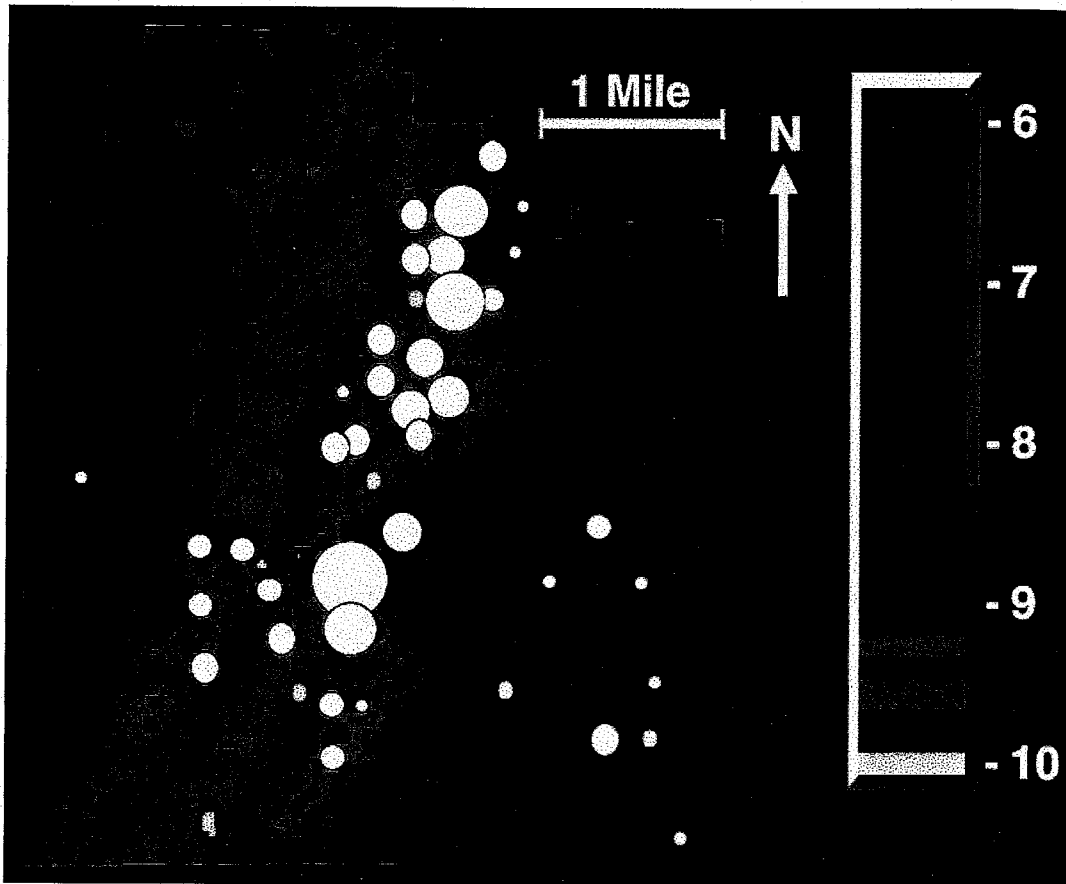


Figure 16: PNN-based average predicted porosity map of the entire units A through D time window with cumulative basal Brushy Canyon production data overlain. We sorted through scout tickets to identify those wells that produce only from the lower Brushy Canyon. The larger bubbles indicate wells with better production. Note that the best production comes from within the channels.

ANALYSIS

The results of this work have implications that go beyond lower Brushy Canyon porosity prediction in this study area. The seismic attribute analyses allow us to gain new

insights into the geology. The results show a more stratigraphically coherent distribution of physical properties than has been previously imaged in the lower Brushy Canyon using seismic attributes (Hardage et al., 1998; Balch et al., 1998). Unlike these two studies, our results show channel-like features of a scale comparable to those mapped in outcrop (Basham, 1996) and in the subsurface (Thomerson and Catalano, 1996). Furthermore, we can show that the best production comes from the stacked channel succession in the center of our study area (Fig. 16).

The PNN model yielded more geologically reasonable results than the linear regression model, but the physics (equation (2)) are much less intuitive. This stresses the need to: a.) examine the physical basis for the seismic attribute selection into the input data before the neural network is even applied, and b.) analyze the results in light of what is known about the geology of the area.

CONCLUSIONS

This project sought to predict the porosity of the lower Brushy Canyon interval in inter-well areas. To do this, we began by evaluating the geology through log-based stratigraphic analysis. The lower Brushy Canyon in this area is characterized by a vertically stacked series of channeled sandstones separated by thin layers of organic siltstones and carbonates. This vertically complex geology caused zones of extreme high and low porosity to appear in the logs. A reliable porosity model had to be able to predict the extreme values, so as to not significantly over-predict the interbeds and under-predict the channel porosity.

We used both linear regression and a neural network in a volume-based approach to model porosity distribution based on seismic attribute analyses. The standard linear

regression model adequately predicted the porosity in areas of greater well control, but failed in areas of sparse well control. As a result, the linear regression model did not accurately portray the channels that we interpreted from well log information.

The probabilistic neural network (PNN) was trained to find the best non-linear relationship between the seven seismic attributes and the actual porosity log. The results were an all around improvement over the regression model. Not only did the PNN yield a higher correlation coefficient, the relationship it found greatly reduced the problem of sparse well coverage. This model also predicted edges of high porosity zones parallel to the interpreted channel boundaries even in areas where there are no wells to constrain the location of the channel.

These results indicate that, when properly employed, neural networks can provide a means of improving subsurface physical property predictions, and avoiding the pitfalls described by Schuelke et al. (1998) and Hart (1999).

REFERENCES

- Bahorich, M., and Farmer, S., 1995, 3-D seismic discontinuity for faults and stratigraphic features: the coherence cube: *The Leading Edge*, v. 14, n. 10, p. 1053-1058.
- Balch, R.S., Weiss, W.W., and Wo, S., 1998, Correlating seismic attributes to reservoir properties using multi-variate non-linear regression, *in* DeMis, W.D., and Nelis, M.K., Eds., *The search continues into the 21st century*, West Texas Geological Society Publication 98-105, p. 199-203.
- Basham, W.L., 1996, Delaware Mountain Group sandstone channel orientations: implications for sediment source and deposition, *in* DeMis, W.D., and Cole, A.G., Eds., *The Brushy Canyon play in outcrop and subsurface: concepts and examples*, Guidebook Permian Basin Section, SEPM, p. 91-102.
- Behnken, F.H., 1996, Reservoir characterization of the Brushy Canyon Formation sandstone (Late Permian), strata production, Nash Unit #15, Nash Draw Delaware Field, Eddy County, New Mexico, *in* DeMis, W.D., and Cole, A.G., Eds., *The Brushy Canyon play in outcrop and subsurface: concepts and examples*, Guidebook Permian Basin Section, SEPM, p. 173-182.
- Bouma, A.H., 1996, Initial comparison between fine- and coarse-grained submarine fans and the Brushy Canyon Formation sandstones, *in* DeMis, W.D., and Cole, A.G., Eds., *The Brushy Canyon play in outcrop and subsurface: concepts and examples*, Guidebook Permian Basin, SEPM, p. 41-50.
- Brown, A.R., 1996, Interpretation of three-dimensional seismic data, fourth edition: AAPG Memoir 42, 424 p.
- Gardner, M.H., and Sonnenfield, M.D., 1996, Stratigraphic changes in facies architecture of the Permian Brushy Canyon in Guadalupe Mountains National Park, West Texas, *in* DeMis, W.D., and Cole, A.G., Eds., *The Brushy Canyon play in outcrop and subsurface: concepts and examples*, Guidebook Permian Basin Section, SEPM, p. 17-40.
- Hampson, D., Schuelke, J., and Quirein, J.A., in press, Using multiattribute transforms to predict log properties from seismic data: Geophysics.
- Hampson and Russell Software Services Ltd., 1998, *Strata Guidebook*, 650 p.
- Hardage, B.A., Simmons Jr., J.L., Pendleton, V.M., Stubbs, B.A., and Uszynski, B.J., 1998, 3-D seismic imaging and interpretation of Brushy Canyon slope and basin thin-bed reservoirs, northwest Delaware Basin: *Geophysics*, v. 63, n. 5, p. 1507-1519.
- Harms, J.C., and Brady, M.J., 1996, Deposition of the Brushy Canyon Formation: 30 years of conflicting hypotheses, *in* DeMis, W.D., and Cole, A.G., Eds., *The Brushy*

Canyon play in outcrop and subsurface: concepts and examples, Guidebook Permian Basin Section, SEPM, p. 51-59.

Hart, B.S., 1998, New Insights on the stratigraphy and production characteristics of the Bone Spring Formation: The Search Continues into the 21st Century, West Texas Geological Society, Publication 98-105, p. 119-126.

Hart, B.S., 1999, Geology plays key role in seismic attribute studies: Oil & Gas Journal, July 12, p. 76-80.

Hart, B.S., and Balch, R.S., 2000, Approaches to defining reservoir physical properties from 3-D seismic attributes with limited well control: and example from the Jurassic Smackover Formation, Alabama: Geophysics, v. 65, n. 2, p. 368-376.

Hirsche, K., Porter-Hirsche, J., Mewhort, L., and Davis, R., 1997, The use and abuse of geostatistics: The Leading Edge, v. 16, n. 3, p. 253-260.

Justman, H., in press, An evaluation of the source rock, reservoir rock, and sequence stratigraphy for the Brushy Canyon Formation's hydrocarbon accumulation in the Delaware Basin, southeast New Mexico, M.S. thesis.

Kalkomey, C.T., 1997, Potential risks when using seismic attributes as predictors of reservoir properties: The Leading Edge, v. 10, n. 1, p. 11-15.

Masters, T., 1995, Advanced algorithms for neural networks: A C++ sourcebook: John Wiley & Sons, Inc., 425 p.

Montgomery, S.L., Worrall, J., and Hamilton, D., 1999, Delaware Mountain Group, west Texas and southeastern New Mexico, a case of refund opportunity: part 1-Brushy Canyon: AAPG Bulletin, v. 83, n. 12, p. 1901-1926.

Pearson, R.A., and Hart, B.S., 1999, Convergence of 3-D seismic attribute-based reservoir property prediction and geologic interpretation as a risk reduction tool: a case study from a Permian intraslope basin: SEG expanded abstracts, p., 896-899.

Ronen, S., Schultz, P.S., Hattori, M., and Corbett, C., 1994, Seismic guided estimation of log properties part 2: using artificial neural networks for non-linear attribute calibration: The Leading Edge, v. 13, n. 6, p. 674-678.

Russell, B., Hampson, D., Schuelke, J., and Quirein, J., 1997, Multiattribute seismic analysis: The Leading Edge, v. 16, p. 1439-1443.

Sageman, B.B., Gardner, M.H., Armentrout, J.M., and Murphy, A.E., 1998, Stratigraphic hierarchy of organic carbon-rich siltstones in deepwater facies, Brushy Canyon Formation (Guadalupian), Delaware Basin, west Texas: Geology, v. 26, n. 5, p. 451-454.

Schuelke, J.S., and Quirein, J.A., 1998, Validation: a technique for selecting seismic attributes and verifying results: SEG, Technical Program Expanded Abstracts with Authors Biographies, Vol. 1, p. 936-939.

Schuelke, J.S., Quirein, J.A. and Sarg, J.F., 1998, Reservoir architecture and porosity distribution, Pegasus Field, west Texas - an integrated sequence stratigraphic - seismic attribute study using neural networks, In: Expanded Abstracts, Geo-Triad, p. 142-145.

Thomerson, M.D., and Catalano, L.E., 1996, Depositional regimes and reservoir characteristics of the Brushy Canyon sandstones, East Livingston Ridge Delaware Field Lea County, New Mexico, *in* DeMis, W.D., and Cole, A.G., Eds., The Brushy Canyon play in outcrop and subsurface: concepts and examples, Guidebook Permian Basin Section, SEPM, p. 103-111.

Yang, K., and Dorobek, S.L., 1995, The Permian Basin of west Texas and New Mexico: tectonic history of a "composite" foreland basin and its effects on stratigraphic development: Stratigraphic Evolution of Foreland Basins, SEPM Special Publication No. 52.

APPENDIX 1

Procedures, Methods, and Applications in Geologic Interpretations

Stratigraphic Interpretations

All stratigraphic interpretations were done in Landmark's Stratworks application. First, lower Brushy Canyon and Bone Spring tops were picked in each of the digitized well logs based on GR, PEF, LLD, and RHOB characteristics. Lower Brushy Canyon pick depths range from 8264 feet in well #7 (Fig.17) to 8435 feet in well #6. Bone Spring pick depths range from 8651 feet in well #9 to 8763.5 feet in well #10 (Table 3). Next, we picked stratigraphic units within the lower Brushy Canyon interval based on log cycles and laterally continuous interbeds. These units were named A through H in descending order and correlated from well to well using tight-boxed cross-sections to ensure the accuracy of the pick from one location to the next in Stratworks' Correlation program. All isopach maps were contoured in Stratworks' Map View and calculated from the stratigraphic top of a lower Brushy unit to the top of the underlying unit.

The top of the lower Brushy Canyon Formation was picked at the top of a maximum flooding surface in the logs between 8250 and 8400 feet at most well locations. At some locations, the lower Brushy top is characterized by carbonate material at similar depths (Fig. 18). This material is typically less than 30 feet thick, and may be seen in the high PEF, LLD, and RHOB log readings. At the base of this carbonate or organic rich siltstone and dolomite material is where the top of Unit A was picked. Unit A generally consists of a relatively thin (20 – 50 feet) massive sandstone, but it is characterized by a coarsening-upwards package towards the east as denoted by a gradual upward decrease in the GR reading (Fig. 18).

| <u>Well #1</u> | <u>Depth(ft)</u> | <u>Time(ms)</u> | <u>Well #2</u> | <u>Depth(ft)</u> | <u>Time(ms)</u> | <u>Well #3</u> | <u>Depth(ft)</u> | <u>Time(ms)</u> |
|-----------------|------------------|-----------------|-----------------|------------------|-----------------|----------------|------------------|-----------------|
| LBC | 8336.5 | 1202.93 | LBC | 8362 | 1211.61 | LBC | 8312 | 1204.26 |
| A | 8352 | 1204.58 | A | 8379.5 | 1214.62 | A | 8334.5 | 1206.62 |
| A lime | 8382 | 1207.78 | A lime | 8415.5 | 1220.82 | A lime | 8377 | 1211.09 |
| B | 8392 | 1208.95 | B | 8422.5 | 1222.02 | B | 8384.5 | 1211.88 |
| C | 8439 | 1213.86 | C | 8475.5 | 1230.71 | C | 8436.5 | 1217.34 |
| C lime | 8517 | 1220.46 | C lime | 8544.5 | 1238.57 | C lime | 8506.5 | 1223.37 |
| D | 8528 | 1221.25 | D | 8551 | 1239.18 | D | 8516.5 | 1224.09 |
| D lime | 8580 | 1225.28 | E | 8605 | 1245.7 | D lime | 8571.5 | 1228.75 |
| E | 8584 | 1225.56 | G | 8684 | 1258.73 | E | 8574.5 | 1229 |
| G | 8652.5 | 1235.08 | H | 8730 | 1263.91 | G | 8648 | 1239.45 |
| H | 8695 | 1241.21 | BSPG | 8763 | 1266.82 | H | 8689 | 1245.71 |
| BSPG | 8731 | 1246.13 | | | | BSPG | 8726 | 1251.36 |
| <u>Well #4</u> | <u>Depth(ft)</u> | <u>Time(ms)</u> | <u>Well #5</u> | <u>Depth(ft)</u> | <u>Time(ms)</u> | <u>Well #6</u> | <u>Depth(ft)</u> | <u>Time(ms)</u> |
| LBC | 8315 | 1202.37 | LBC | 8380 | 1209.69 | LBC | 8435.5 | 1209.79 |
| A | 8334 | 1205.02 | A | 8400.5 | 1212.38 | A | 8453 | 1211.89 |
| A lime | 8365.5 | 1209.43 | A lime | 8418.5 | 1215.17 | A lime | 8466.5 | 1213.5 |
| B | 8377 | 1211.04 | B | 8433 | 1217.07 | B | 8480.5 | 1214.69 |
| C | 8425.5 | 1217.82 | B lime | 8479 | 1223.76 | C | 8515 | 1217.46 |
| C lime | 8498.5 | 1226.48 | C | 8490 | 1225.13 | C lime | 8569.5 | 1221.84 |
| D | 8506 | 1227.02 | F | 8534.5 | 1232.06 | F | 8577 | 1222.44 |
| E | 8555.5 | 1230.57 | E | 8562 | 1235.28 | E | 8612 | 1226.94 |
| G | 8626.5 | 1237.99 | G | 8656.5 | 1243.76 | H | 8684 | 1237.37 |
| H | 8670.5 | 1243.67 | H | 8674 | 1245.22 | BSPG | 8713 | 1241.57 |
| BSPG | 8704.5 | 1248.08 | BSPG | 8701 | 1248.39 | | | |
| <u>Well #7</u> | <u>Depth(ft)</u> | <u>Time(ms)</u> | <u>Well #8</u> | <u>Depth(ft)</u> | <u>Time(ms)</u> | <u>Well #9</u> | <u>Depth(ft)</u> | <u>Time(ms)</u> |
| LBC | 8264 | 1208.26 | LBC | 8301.5 | 1209.39 | LBC | 8268.5 | 1206.77 |
| A | 8284 | 1210.78 | A | 8326 | 1212.72 | A | 8289 | 1209.15 |
| A lime | 8325 | 1215.95 | A lime | 8366 | 1218.02 | B | 8349.5 | 1216.18 |
| B | 8331 | 1216.7 | B | 8378 | 1219.78 | C | 8384 | 1220.19 |
| C | 8385 | 1223.51 | B lime | 8411 | 1224.26 | C lime | 8449.5 | 1227.81 |
| C lime | 8457 | 1232.58 | C | 8424.5 | 1226.09 | D | 8470.5 | 1231.35 |
| D | 8478.5 | 1234.86 | C lime | 8490.5 | 1233.53 | E | 8515 | 1236.8 |
| E | 8513.5 | 1237.83 | D | 8505.5 | 1234.62 | G | 8570.5 | 1243.59 |
| G | 8573.5 | 1242.91 | D lime | 8517.5 | 1235.55 | H | 8605.5 | 1248.54 |
| H | 8615.5 | 1248.48 | E | 8534.5 | 1236.87 | BSPG | 8651.5 | 1253.87 |
| BSPG | 8652 | 1254.05 | G | 8611 | 1244.35 | | | |
| | | | H | 8641.5 | 1248.6 | | | |
| | | | BSPG | 8669 | 1252.67 | | | |
| <u>Well #10</u> | <u>Depth(ft)</u> | <u>Time(ms)</u> | <u>Well #11</u> | <u>Depth(ft)</u> | <u>Time(ms)</u> | | | |
| LBC | 8346 | 1204.35 | LBC | 8343.5 | 1212.05 | | | |
| A | 8365.5 | 1206.53 | A | 8362 | 1214.1 | | | |
| A lime | 8402.5 | 1210.67 | A lime | 8391.5 | 1217.38 | | | |
| B | 8409.5 | 1211.46 | B | 8397.5 | 1218.04 | | | |
| C | 8463.5 | 1217.5 | C | 8439 | 1222.64 | | | |
| C lime | 8537 | 1223.19 | C lime | 8525 | 1230.11 | | | |
| D | 8548 | 1224.02 | D | 8535 | 1230.85 | | | |
| E | 8596 | 1228.24 | E | 8574 | 1233.76 | | | |
| G | 8685.5 | 1242.77 | G | 8669.5 | 1244.9 | | | |
| H | 8728.5 | 1250.81 | H | 8717.5 | 1250.52 | | | |
| BSPG | 8763.5 | 1256 | BSPG | 8749 | 1253.73 | | | |

Table 3: Time/depth pairs for every lower Brushy Canyon stratigraphic pick for each of the 11 wells in the multiattribute study. The locations of these wells are given in Figure 17. LBC is the lower Brushy Canyon. BSPG is the Bone Spring Formation.

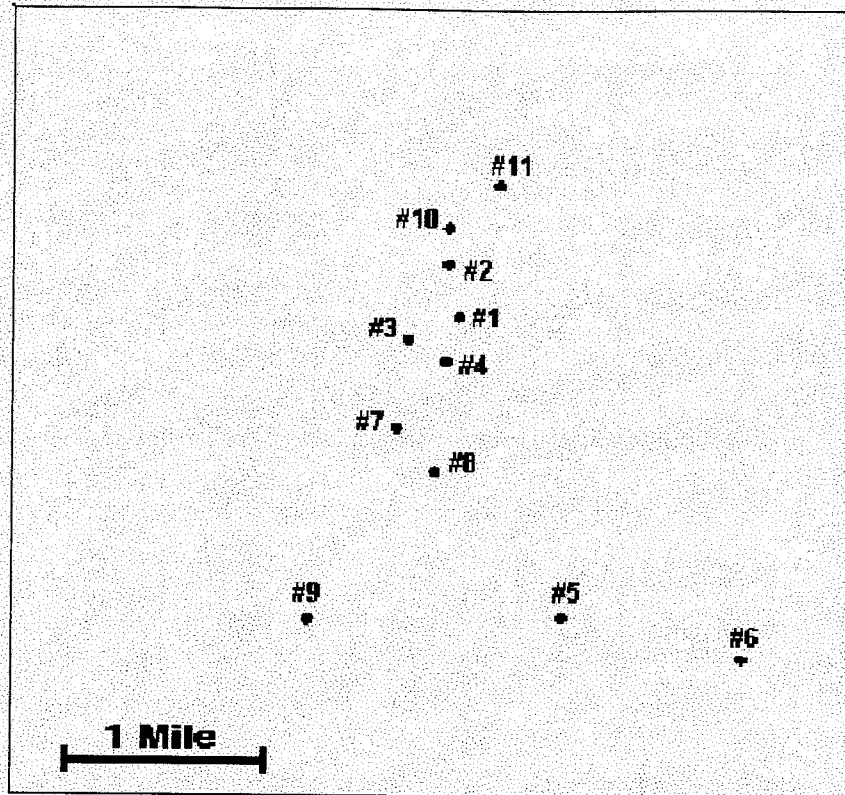


Figure 17: Locations of the 11 wells used in the multiattribute study. Refer also to the white dots in Figure 15.

Either a thin organic rich siltstone/dolomite or a carbonate layer vertically separates Unit A from Unit B (called A lime). This laterally extensive boundary proved to be an excellent marker bed with which to separate the two units. Unit B consists of a massive sandstone (relatively flat GR response) in most areas, but, similar to Unit A, it changes to a coarsening-upwards package to the east.

Again, a laterally equivalent bed of either organic siltstone/dolomite or a limestone proved to be an excellent marker bed with which to vertically separate Unit B from Unit C (called B lime). Unit C was very easy to correlate from well to well as it is the thickest, cleanest, and most productive unit in the lower Brushy Canyon in this study area.

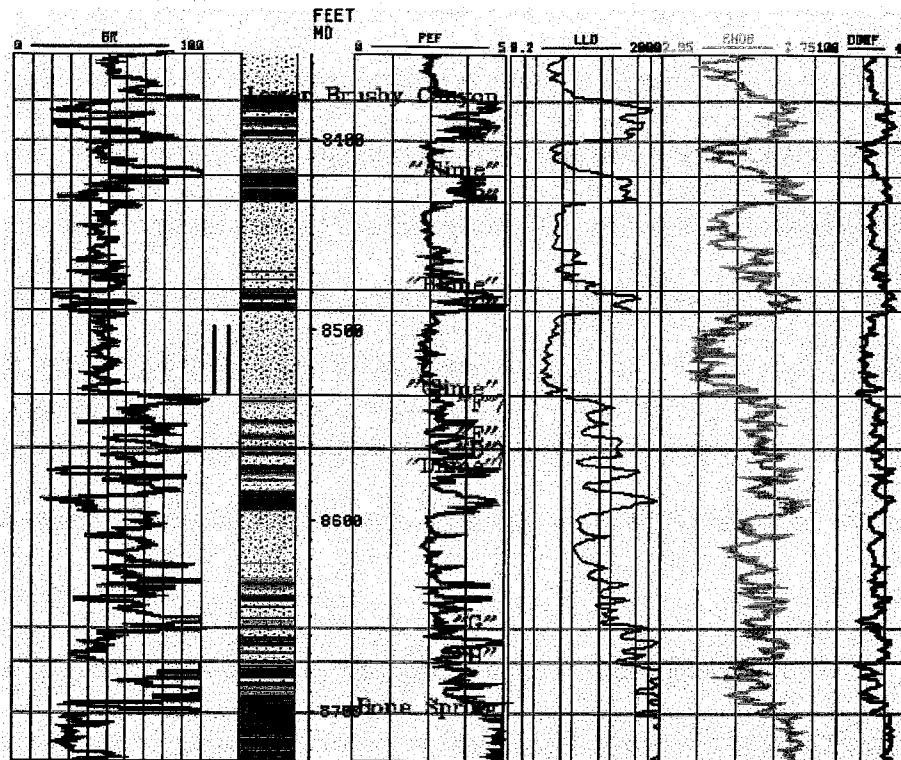


Figure 18: Well logs and log-based lithology column of a well southeast of center in the study area. The logs are, from left to right: the GR, PEF, deep resistivity (LLD), RHOB, and the sonic (DT) logs. The lithology column is log-derived, based on sand/shale lines and carbonate lines using the GR and PEF logs. To the left of the column is an engineering track showing perforation zones.

At the base of Unit C is another thin bed of organic siltstone/dolomite or limestone (called C lime). This thin bed was laterally extensive throughout the study area, and again proved to be a reliable pick to vertically separate Unit C from the underlying unit. In the center of the study area, the unit beneath Unit C is Unit D. Unit D is a channeled sandstone that cuts through the organic siltstone/dolomite of Unit F. Unit D may be seen on the type log (Fig. 2), and Unit F may be seen here on Figure 18. Every log in the study area had either a Unit D or a Unit F pick as the two are stratigraphically equivalent (Fig. 19).

In wells where Unit D is present, Unit E lies directly beneath either another organic siltstone/dolomite or a carbonate bed at the base of Unit D (called D lime). Wells where Unit F is present tend to show a gradual shift into Unit E as log characteristics are similar (a package of relatively high GR readings). In this case, Unit E was picked at the top of a fining-upwards package, which was correlated with the top of Unit E in wells that contained Unit D. Unit E was the toughest unit to correlate due to internal stratigraphic variation from well to well. It mostly consists of a massive sandstone in the western region, a coarsening-upwards to fining-upwards package in the center, and a carbonate towards the east.

Unit G underlies Unit E in most wells, although pinchouts do occur (Fig. 19). The top of Unit G is characterized by an abrupt kick to the left in the GR curve (Fig. 18). This unit generally consists of a massive sandstone in the west (with low porosity) and a carbonate to the east. This was determined from the relatively high (around 5) reading on the PEF curve.

Unit H is the lowest unit stratigraphically in the lower Brushy in this study area. It consists of mostly organic-rich carbonates as seen from the high GR and high PEF readings.

Synthetic Seismograms

Upon determining a stratigraphic model for the lower Brushy Canyon Formation in this study area, our next goal was to accurately tie the stratigraphic picks on the well logs to the seismic data. This was done by way of synthetic seismograms (Fig. 20). All final synthetics were generated in Hampson and Russell's Strata program (Landmark's PostStack PAL program was needed to convert the .3dv volume to a SEG-Y volume that

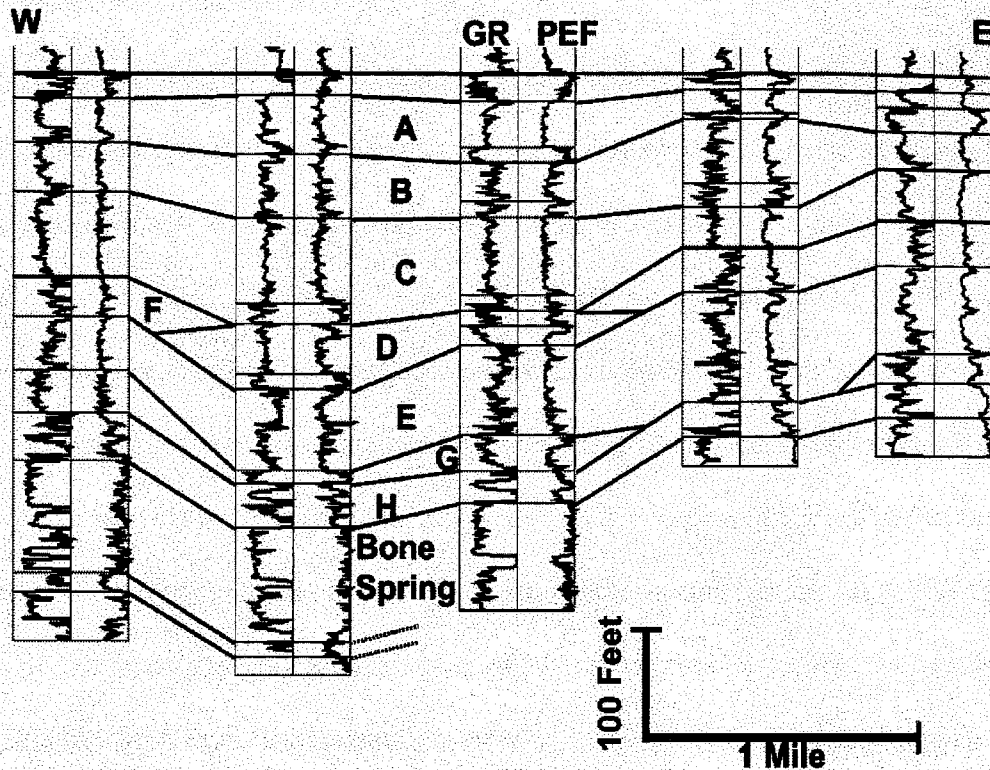


Figure 19: A west – east cross-section showing basic lower Brushy Canyon stratigraphy. The logs used are the GR and the PEF log from left to right. Note the stratigraphic equivalent Units D and F, and the pinchout of Unit G in the second well from the right.

Strata would recognize). This software package looks at the sonic (DT) and density (RHOB) logs to determine the acoustic impedance. Once this is determined, the software generates a synthetic or model of what a seismic trace should look like that travels through that particular section of rock. The section we are interested in is the lower Brushy Canyon interval, but an accurate synthetic will tie log data and seismic data over a much larger window. The thickness (in time) of the lower Brushy ranges from 32 to 56 ms in the 11 wells used in the multi-attribute study (Table 3). These wells were accurately tied to the seismic data over a window of at least 500 ms. Wells typically tied

as far up in the log as the Bell Canyon Formation and as far down as the Wolfcamp (depending on the total depth of the well).

First, sonic and density logs were input into Landmark's Syntool program. Syntool was used as a first step to get the wells tied over a bigger time interval before fine-tuning them in Strata. Syntool will generate a synthetic and overlay it on seismic traces imported in SEG-Y format. For the first well, we did not apply a time-depth table. Since the sonic logs did not start at the surface, the software had to estimate a constant velocity from the surface to the starting depth of the log. Because of this, we had to apply a visually estimated time shift to get started. Syntool will then display the amount of time to further shift the log to best match the synthetic curve to the seismic data.

After the time shift had been applied, we needed to adjust the phase of the synthetic to match the seismic data. Syntool will display the degrees out-of-phase at the bottom of the correlation window. This can be adjusted in the filter window. Once the appropriate phase shift was applied, the frequency filter could be adjusted to match the frequency of the seismic data. This varied from well to well. The default filter is a trapezoid filter with frequency ranges of 8-14-40-60 for the low cut, low pass, high pass, and high cut respectively. Our frequencies were typically in the 15 to 50 Hz range.

The next step was to extract a mixed phase wavelet from the seismic data following the methods of Hampson and Russell (1998). This will better match the characteristics of the synthetic to the seismic data to yield a higher correlation coefficient. The correlation coefficient was used to measure the accuracy of the well – seismic tie. A correlation coefficient of 1.0 would mean a perfect correlation. For the 11 wells used in the attribute study, the correlation coefficients ranged from 0.628 to 0.907 (Table 4). Due

to the wavelength of the data, only wavelets of at least 400, preferably 500, ms were extracted. This correlates to approximately 3000 feet of rock, depending on lithology, so only those wells with logs containing more than 3000 feet were used. Also, the correlation time window could be changed to alter the correlation coefficient. This is the time window in which the correlation coefficient is calculated. It is independent of the window of wavelet extraction, but should fall within. Generally, the smaller the window, the better the correlation, but windows of at least 500 ms were desired here to show that the correlation was good over as large a time window as possible

Since our seismic data were sampled at every 2 ms, it was necessary to accurately tie the well log to the seismic at every sample to later perform the volume-based multi-attribute study. The capabilities of the Strata program allowed us to stretch and squeeze the synthetics where necessary and to extract a wave from the seismic data to increase the correlation.

| <u>Well Number</u> | <u>Wavelet Extraction Window</u> | <u>Correlation Window</u> | <u>Correlation Coefficient</u> |
|--------------------|----------------------------------|---------------------------|--------------------------------|
| 1 | 900 - 1400 ms | 900 - 1400 ms | 0.628 |
| 2 | 800 - 1370 ms | 860 - 1290 ms | 0.907 |
| 3 | 850 - 1350 ms | 1040 - 1400 ms | 0.836 |
| 4 | 810 - 1260 ms | 1000 - 1260 ms | 0.769 |
| 5 | 900 - 1310 ms | 1000 - 1310 ms | 0.845 |
| 6 | 865 - 1275 ms | 865 - 1275 ms | 0.691 |
| 7 | 812 - 1262 ms | 874 - 1262 ms | 0.826 |
| 8 | 850 - 1262 ms | 850 - 1262 ms | 0.779 |
| 9 | 900 - 1400 ms | 920 - 1340 ms | 0.761 |
| 10 | 780 - 1420 ms | 780 - 1420 ms | 0.876 |
| 11 | 840 - 1290 ms | 840 - 1290 ms | 0.907 |

Table 4: List of the correlation coefficients and time windows for each of the wells used in the multiattribute study. Well locations are shown in Figure 17.

Seismic Interpretations

Once the wells containing DT and RHOB logs were accurately tied to the seismic, we could begin to track horizons in the seismic data. A peak in the seismic at around 1200 ms correlated to the top of the lower Brushy Canyon. This peak was auto-tracked through the entire seismic data as the lower Brushy top (Fig. 21). The Bone Spring was characterized as a peak at about 1250 ms (Fig. 22). In some areas, however, excessive carbonate material was deposited on top of the Bone Spring, which threw off the seismic response of the reflector. Nevertheless, the Bone Spring is characterized as a peak throughout most of the study area. Most of the stratigraphic units within the lower Brushy Canyon Formation did not regularly correspond to a peak or a trough due to the thinness of the unit and its relative acoustic impedance with adjacent units. The only exception is Unit C, which is characterized as a trough at about 1220 ms throughout the data set.

All seismic horizon interpretations were done in Landmark's Seisworks application. This program allowed us to pick a grid of seed lines for each horizon, and then auto-track, or interpolate, the horizons over an area in the seismic data. We could then create isochron maps between horizons (Fig. 23). This was done by calculating the time (in ms) difference between the Bone Spring and the lower Brushy Canyon reflection. An isochron of the lower Brushy interval reveals a time thickness range of 32 to 56 ms. The thickest areas in time correlate to the thickest areas in feet as shown on an isopach map. This gave us added confidence that our well logs were accurately tied to the seismic data. This tie is necessary before performing any attribute analyses.

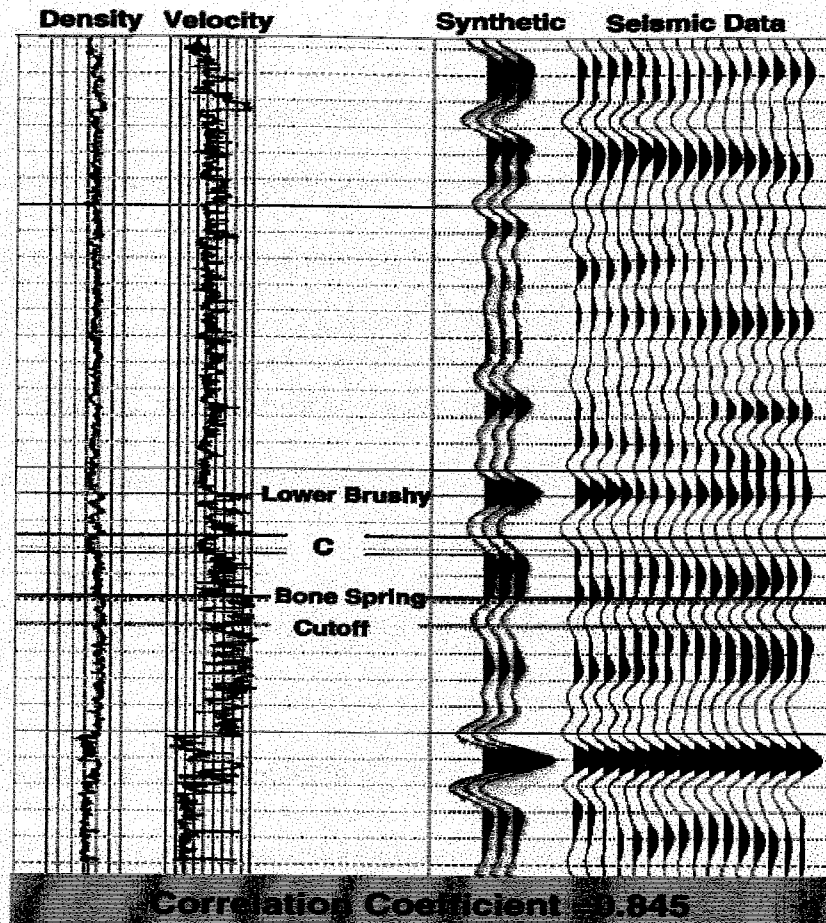


Figure 20: A synthetic seismogram tying the well log to the seismic data. The logs are the RHOB and the sonic velocity log. The blue trace represents the synthetic and the black traces are the actual seismic data. Note the precise tie within the lower Brushy Canyon interval and the good tie well above and below the interval. This precision is needed to perform the following multi-attribute analyses.

Seismic Attribute Analysis

Seismic data is made up of three domains: amplitude, phase and frequency. Most seismic attributes are variations within either of these domains. All seismic attribute analyses were done in Hampson and Russell's Emerge program. This software calculates

17 attributes from the seismic data, and allows external attributes to be imported for analysis as well. The smoothed acoustic impedance was calculated in Hampson and Russell's Strata program following Hampson and Russell (1998). This was done as a blocky inversion over a 400 ms (1000 – 1400 ms) time window using the average extracted wave from the 11 wells used in the study. The minimum continuity volume was created in Landmark's PostStack PAL program (F-Scan 3-D). Other attributes we calculated in PostStack were the energy half-time, and the arc length. Neither of these attributes were chosen by step-wise regression, but the physical basis for using them was deemed based on their equations. Each of these additional attributes needed to be converted into SEG-Y format before use in Emerge. This was also done in PostStack. Because SEG-Y files take up so much disk space, these attributes were only extracted over a 400 ms time window as opposed to over the entire seismic volume.

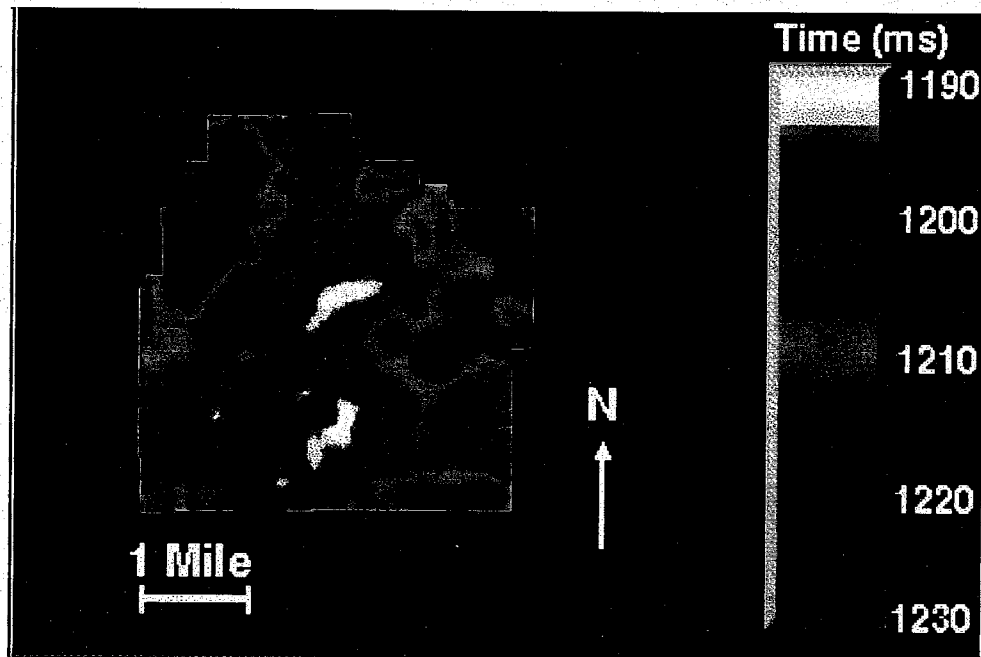


Figure 21: Time-structure map the lower Brushy Canyon Formation as interpreted in the seismic volume. The depth in time is given in ms in the legend. Note the high structure in the center of the study area. This is from the accumulation of sand from the vertically stacked channels in this region.

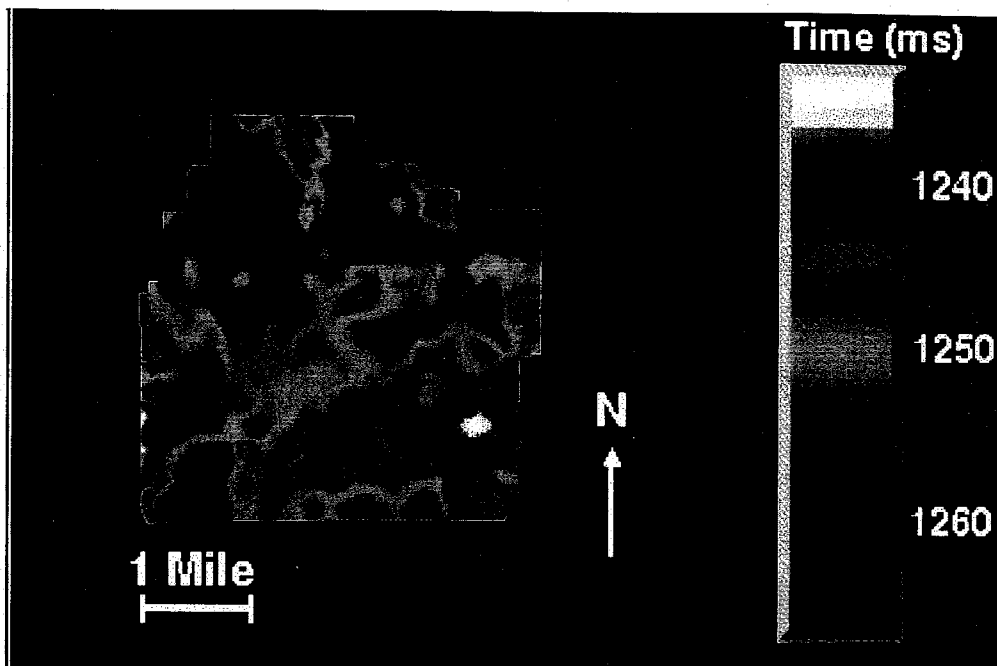


Figure 22: Time-structure map of the top of the Bone Spring horizon in the seismic data. The depth is in time and is given in ms in the legend. Note the high structural mound in the southeast. This feature is seen in the depth converted structure map (Fig. 6).

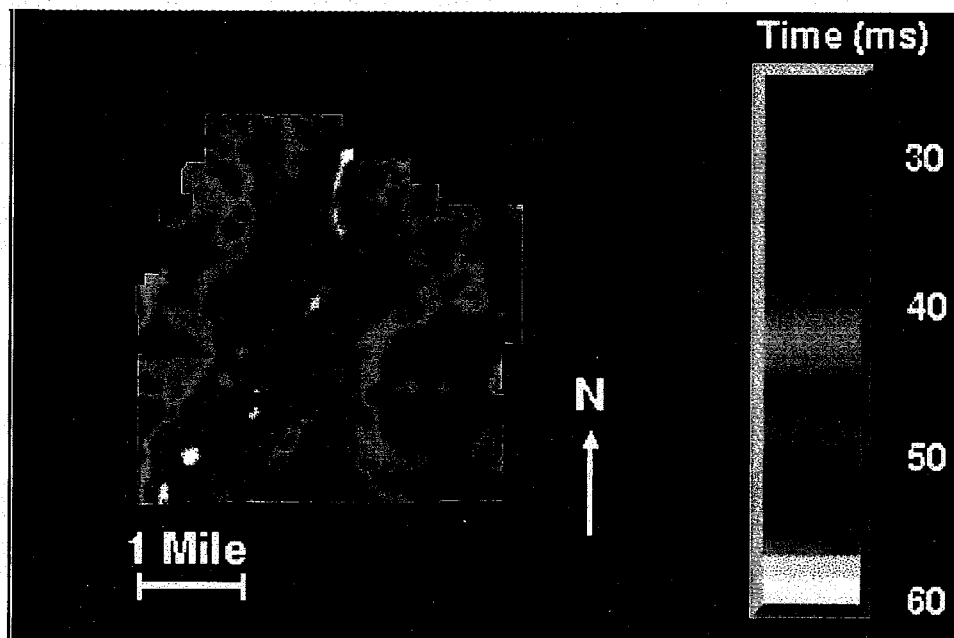


Figure 23: Isochron of the lower Brushy Canyon interval in the seismic volume. Thickness is measured in ms and is given in the legend. Note the north – south thick trend in the center of the study area. This is showing the accumulation of sand from the vertically stacked channels.

The attributes were first individually cross-plotted with neutron porosity, and the correlation coefficients were noted. The blocky inversion, or seismic acoustic impedance, correlated best with neutron porosity, but as stated above it could not be used solely as a seismic attribute since it is log influenced. However, all of the wells were time shifted to maximize the correlation of the inversion. This fine-tuned the wells in the

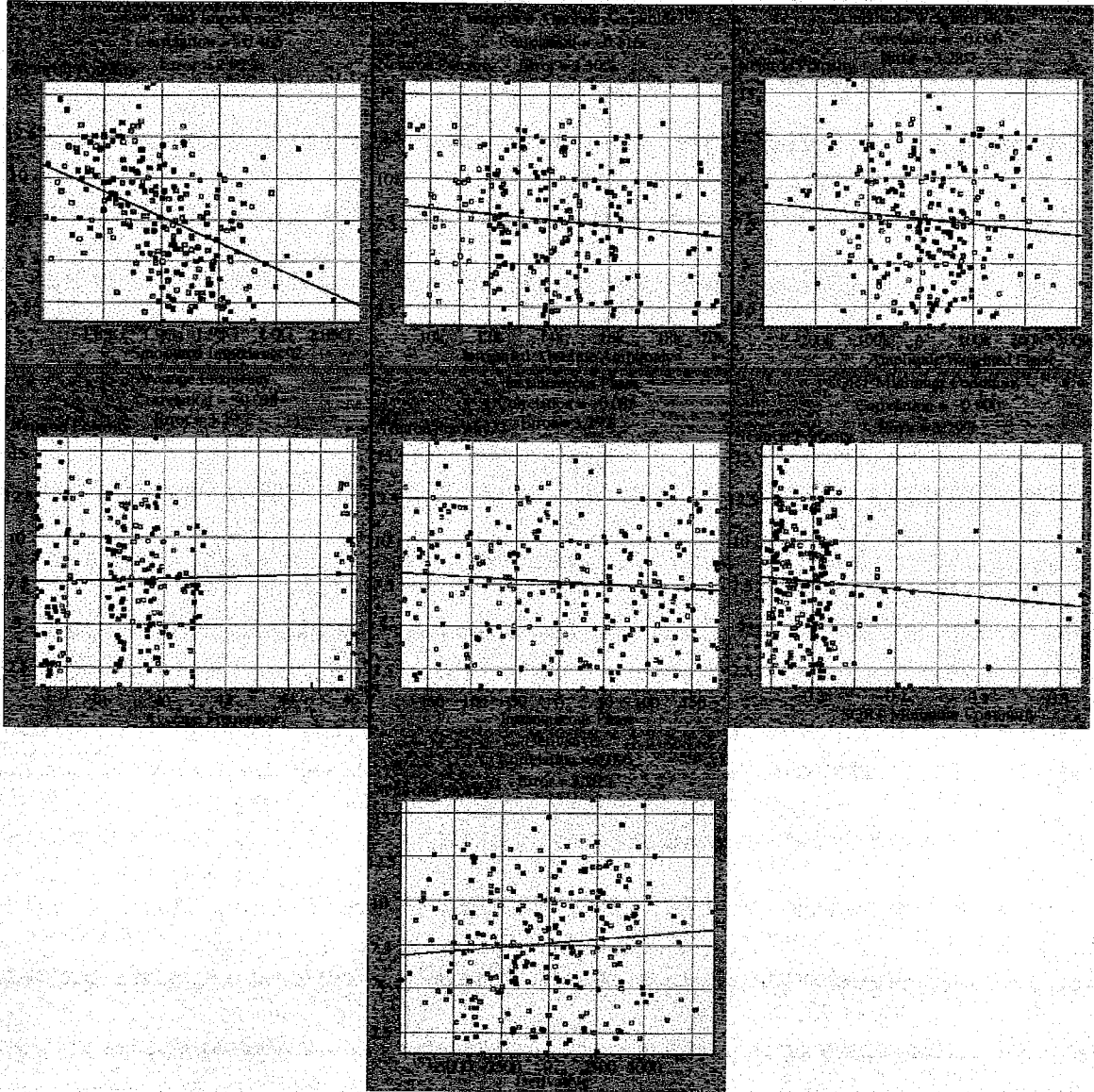


Figure 24: Individual cross-plots of attribute vs. neutron porosity for each of the seven attributes used in the analysis. Note the low correlation coefficients in each case when only one attribute is used to predict the porosity.

seismic data to the best tie at each sample point. Even though the inversion could not be used in the multiattribute study, it was used to aid in the tying of the well data, which increased the individual correlations of the other attributes. The individual correlation coefficients were typically very poor (the highest being Smoothed Impedance² at $r=0.47$ and the lowest approaching 0 correlation) by themselves (Fig. 24).

The attribute with the highest correlation coefficient is ranked number one. The remaining attributes are subsequently ranked by their ability to assist the number one attribute in lowering the average regression error. This process is called step-wise regression. The result is a list of as many attributes as the software will extract from the seismic data, with a reduced error as each attribute is added to the list.

There is a maximum number of attributes to use. The process of validation informed us that 7 attributes were necessary to best predict the neutron porosity. This process leaves one well out at a time for prediction based on the other wells in the training set. This is a controlled test that allows us to validate the predictive power of the chosen attributes. As attributes are added and combined, the error will decrease until a certain point at which the attributes become too well-specific and cannot accurately predict at another well location outside the training set. The attribute that is added to give the lowest validation error is the last attribute that may be used in the analysis. The operator length was set at five for this experiment. This averages the attribute values in the seismic data over a window of five samples to predict at each sample in the log (Hampson et al., in press). The defaults were used for all other parameters except the integrate length (40 ms).

The first technique we employed to model porosity was standard linear regression. Details of this method are given in Masters (1995). Once the criteria of which attributes to use and how many were determined by the methods described above, the attribute values of the training data were used to determine the regression equation (equation 1). This equation was then used to predict porosity at other locations in the study area. Weights were applied in the slope position of the equation to get the output number in porosity units (i.e. percent units). For example, acoustic impedance, which is on the order of 10^4 would have a weight on the order of 10^{-3} applied to get the output to the order of 10%. The weights are given in Table 5 along with the constant.

| <u>Attribute</u> | <u>Weight</u> | <u>Attribute</u> | <u>Weight</u> |
|-------------------------------|---------------|-------------------------|---------------|
| Smoothed Inversion^2 | -2.20044E-07 | Instantaneous Phase | -0.00732305 |
| Smoothed Inversion^2 | 9.33039E-07 | Instantaneous Phase | -0.00615510 |
| Smoothed Inversion^2 | -1.58664E-06 | Instantaneous Phase | 0.00768994 |
| Smoothed Inversion^2 | 1.50134E-06 | Instantaneous Phase | 0.00182539 |
| Smoothed Inversion^2 | -6.53165E-07 | Instantaneous Phase | -0.14203500 |
| Integrated Absolute Amplitude | 0.00162035 | SQRT Minimum Continuity | 13.05430 |
| Integrated Absolute Amplitude | -0.00147428 | SQRT Minimum Continuity | -28.16500 |
| Integrated Absolute Amplitude | 0.00137865 | SQRT Minimum Continuity | 16.16290 |
| Integrated Absolute Amplitude | -0.00307722 | SQRT Minimum Continuity | 6.46263 |
| Integrated Absolute Amplitude | 0.00189492 | SQRT Minimum Continuity | -4.78472 |
| Amplitude Weighted Phase | 5.69342E-07 | Derivative | 0.00139987 |
| Amplitude Weighted Phase | 1.29252E-06 | Derivative | -0.00486141 |
| Amplitude Weighted Phase | -7.45931E-07 | Derivative | 0.00804671 |
| Amplitude Weighted Phase | -2.23499E-07 | Derivative | -0.00607878 |
| Amplitude Weighted Phase | 1.57712E-06 | Derivative | 0.00209453 |
| Average Frequency | 354.593 | Constant | 30.1649 |
| Average Frequency | -803.984 | | |
| Average Frequency | 161.667 | | |
| Average Frequency | 655.955 | | |
| Average Frequency | -367.817 | | |

Table 5: List of the weights applied to each attribute. Also shown is the constant in the linear regression equation. Each attribute has five weights because the operator length is five. Each attribute value is thus multiplied by each of the five pertaining weights and summed. This value is then entered into equation 1 and is repeated for each of the seven attributes. The constant is then added, and the output value is the predicted porosity at a given sample point.

We then employed the PNN in the same manner to predict porosity using a non-linear approach (see Appendix 2 for details). After both techniques were used to create a porosity model, we could then predict porosity over the entire lower Brushy Canyon interval in the seismic data. The two porosity volumes were created in Emerge. It was then necessary to change the IBM 32-bit floating point SEG-Y format of the seismic data in Emerge to a .3dv file that Landmark would recognize. This was done in PostStack PAL, and the volumes were then imported into Seisworks for seismic display and interpretation. Before making any map views in the porosity volumes it was necessary to extract attributes along a seismic horizon or window. This was done in StratAmp. This allowed us to display porosity values in map view. Because the top of Unit C is the only lower Brushy Canyon horizon we could track in the seismic data, we had to estimate the locations of other horizons in order to generate the porosity maps. For example the maps in Figures 11 and 13 were generated by taking the average porosity of the window from the C horizon to a parallel horizon 9 ms below. This window was estimated based on the data in Table 3. The maps of the lower Brushy units A through D in Figures 12 and 14 were generated over the window from the lower Brushy Canyon horizon to a parallel horizon 30 ms below. In Figure 15, Unit D was estimated to be in the window from the parallel horizons Unit C plus 9 ms to Unit C plus 15 ms.

APPENDIX 2

Definition, Application, and Methodology of the PNN

$$L' = \frac{\sum_{i=1}^n L_i \exp(-D(x, x_i))}{\sum_{i=1}^n \exp(-D(x, x_i))} \quad (2)$$

Definition of the PNN

The mathematics behind the PNN is given in Equation (2). In this equation, L is the predicted value of neutron porosity at any given sample point in the seismic volume. The value of n is the number of training points in the training set. This is given as the sum of all seismic samples within the window of interest (WOI) at each well. For example, a training set with 10 wells and a WOI of 50ms in each well, sampled at every 2ms, would yield an n value of 250. L_i is the actual log-derived porosity value at an individual training point. The expression $-D(x, x_i)$ is the multi-dimensional, or Euclidean,

$$-D(x, x_i) = \sum_{j=1}^7 \left(\frac{x_j - x_{ij}}{\sigma_j} \right)^2 \quad (3)$$

distance between the input point and each of the training points, and is defined in equation (3).

Here, the variable j refers to each individual seismic attribute. In this case, 7 seismic attributes were used in the equation. x_j is the numerical value of each attribute (j) at the location of the input point (the point at which the porosity is to be predicted). x_{ij} is the numerical value of each attribute (j) at the location of each training point (i). The variable σ_j is the smoothing parameter. This parameter is essentially the radius of a bell curve around each training point. This radius is determined by the software by the

process of validation, and it is used to determine the weight assigned to each training point. These values are given in table 6. In summary, the closer the attribute value of an input point is to the attribute value of a training point, the greater that training point will be weighted in the porosity prediction of the input point.

| Attribute | Sigma | Attribute | Sigma |
|-------------------------------|--------------|-------------------------|--------------|
| Smoothed Inversion^2 | 0.2027284267 | Instantaneous Phase | 0.208855717 |
| Smoothed Inversion^2 | 1.4199470695 | Instantaneous Phase | 2.336766583 |
| Smoothed Inversion^2 | 1.6915370842 | Instantaneous Phase | 2.401422952 |
| Smoothed Inversion^2 | 1.8214523305 | Instantaneous Phase | 3.034134699 |
| Smoothed Inversion^2 | 1.9432241511 | Instantaneous Phase | 2.938657647 |
| Integrated Absolute Amplitude | 2.4517021069 | SQRT Minimum Continuity | 1.740159102 |
| Integrated Absolute Amplitude | 2.3179706095 | SQRT Minimum Continuity | 1.633219927 |
| Integrated Absolute Amplitude | 2.3940202022 | SQRT Minimum Continuity | 2.030150413 |
| Integrated Absolute Amplitude | 2.6502264368 | SQRT Minimum Continuity | 2.070806944 |
| Integrated Absolute Amplitude | 2.8775218608 | SQRT Minimum Continuity | 1.820481520 |
| Amplitude Weighted Phase | 1.1731631196 | Derivative | 1.427516574 |
| Amplitude Weighted Phase | 0.5309439875 | Derivative | 1.628692820 |
| Amplitude Weighted Phase | 1.2355418908 | Derivative | 2.147438113 |
| Amplitude Weighted Phase | 2.7116294215 | Derivative | 0.224656397 |
| Amplitude Weighted Phase | 1.3841693286 | Derivative | 1.143277093 |
| Average Frequency | 1.7085301480 | Global Sigma | 1.066666668 |
| Average Frequency | 1.7017318337 | | |
| Average Frequency | 1.6935195564 | | |
| Average Frequency | 1.6838092387 | | |
| Average Frequency | 1.6731581328 | | |

Table 6: List of the sigma values for each attribute. There are five sigmas listed for each attribute because the operator length is five.

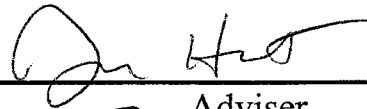
Procedures in Application and Methodology of the PNN

Before employing the PNN, it is necessary to first apply the processes of step-wise regression and validation to the attributes extracted from the seismic data. This will determine which attributes to use, and how many. Once these variables are determined, the PNN may then be applied. The Emerge program will also employ a multi-layered feed-forward neural network (MLFN), but the more easily understandable mathematics

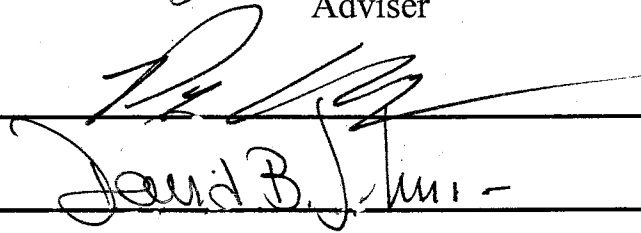
of the PNN made it more desirable than the MLFN, which tends to be more of a "black box".

Upon training the PNN, the software will include only the attributes selected by step-wise regression and validation, and determine the optimal σ_j value by validation. The result of the training will be a model of a non-linear relationship between the log-derived porosity and the seismic attributes based on all training points in the training set. This model may then be applied to the entire seismic volume within the WOI. In creating this predicted porosity volume, the PNN compares the numerical attribute values at every sample point within the WOI to the attribute values at each training point. Training points with attribute values a great distance away from the value at an individual input point will be essentially ignored, as greater weight is given to those training points with similar attribute values to those at the input point. For this reason, it is necessary to have a training set that is representative of each facies in the study area.

This thesis is accepted on behalf of the faculty of the
Institute by the following committee:



Adviser



David B. Jones

8/3/00

Date